Final Report of the HyPER Harvester Project

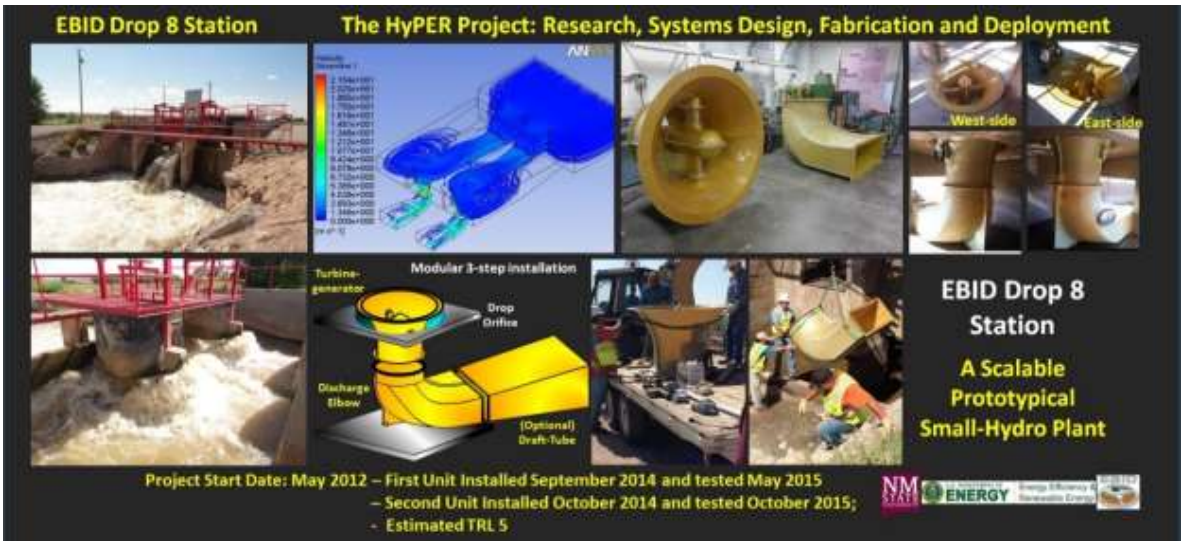

Submitted by

Nadipuram R. Prasad, PI naprasad@nmsu.edu

Satish J. Ranade, Co-PI sranade@ad.nmsu.edu

Klipsch School of Electrical & Computer Engineering
New Mexico State University
Las Cruces, NM 88003-8001

Partner with
Southern New Mexico Elephant Butte Irrigation District (EBID)
Las Cruces, NM 88005

Project funded by
U.S. Department of Energy, Contract DE-EE0005411

Period of performance
May 2012 – October 30, 2015

Submitted to
DOE Wind and Water Power Program

November 30, 2015

Table of Contents **Page**

Cover Picture Theme: "*Where there is water there is power*"

Graphic shows 1) the historic Drop 8 Station with two, 2-meter drops through circular orifices with the potential for approximately 30kW per drop, 2) a 3D fluid dynamic simulation illustrating flow conditions during maximum flow through a model of the Drop 8 Station, 3) the design concept illustrating modularity and the effect of scalability that allows "custom-fitting" of a drop site and the ease of installation, 4) a complete prototype showing the plug-&-play modularity and awaiting transport from MTEC, the manufacturing center at New Mexico State University, to EBID Drop 8 Station for deployment, 5) demonstrating the ability for rapid installation with minimum crew and equipment due to light weight modular components, 6) East-side and West-side units each installed in less than 1 Hour. The graphic epitomizes the ease of manufacturability and deployment. Collectively, these attributes make it a least cost technology for low-head hydropower. Note from PI: A prototype of this magnitude offered no hope for an alternate means for testing due to the large volume of water required. Laboratory testing was ruled out. Out of the curiosity to find a quote that matched exactly with the selected theme "*Where there is water there is power*", the search led to the script of a 1930 film "The River", produced by the U.S. Department of Agriculture, which describes the Mighty Mississippi River as a grand natural renewable resource for power generation. It serves to inspire the continued development of hydropower in ways that preserve the ecology and the environment.

Acknowledgment: This material is based upon work supported by the Department of Energy under Award Number DE-EE0005411.

Disclaimer: "This report was prepared as an account of work sponsored by an agency of the United States Government. Neither the United States Government nor any agency thereof, nor any of their employees makes any warranty, express or implied, or assumes any legal liability or responsibility for the accuracy, completeness, or usefulness of any information, apparatus, product or process disclosed, or represents that its use would not infringe privately owned rights. Reference herein to any specific commercial product, process or service by trade name, trademark, manufacturer, or otherwise does not necessarily constitute or imply its endorsement, recommendation, or favoring by the United States Government or any agency thereof. The views and opinions of authors expressed herein do not necessarily state or reflect those of the United States Government or any agency thereof."

Summary of the HyPER Harvester Project: Innovation for low-head hydropower

Technology at a glance

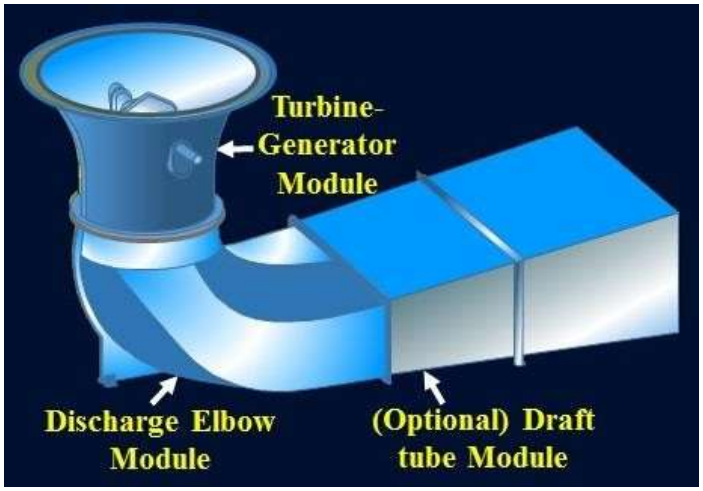

Key Harvester Attributes
Modular, Plug-&-Play
Carbon-composite and Fiberglass shell
Light weight composite impeller
Easy to fabricate
Easy to assemble
Easy to deploy
Highly durable
Self-supporting structure
Low manufacturing cost
Minimally intrusive
Environmentally aesthetic
Scalable and Custom-engineered to fit

Using additive manufacturing techniques, the harvester is fabricated with Carbon-composites and Fiberglass to provide high tensile and compression strength properties to the modular elements. The hand-crafted modular turbine components include:

1) a Venturi-turbine fabricated as two axially-symmetric half-moldings
2) a submarine fabricated as two axially-symmetric half-moldings,
3) a discharge elbow fabricated as two mirror-symmetric half-moldings, and
4) a Carbon-composite impeller (hub and blades) with a Steel shaft

Steel shafts of the impeller and generator/alternator are coupled by a Steel coupler and supported vertically by the submarine with a suitable thrust bearing. **Complete harvester assembly ~5 hours**

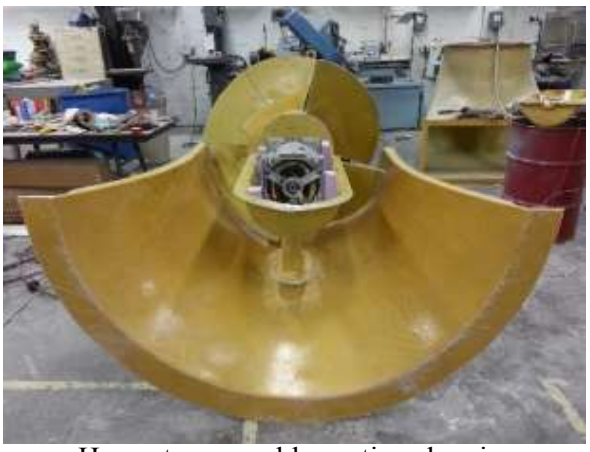

Harvester assembly section showing generator and impeller in composite half-moldings of submarine and the Venturi

Fully assembled harvester turbine-generator & discharge modules at NMSU-MTEC awaiting deployment at EBID Drop 8 Station

Ease of Deployment

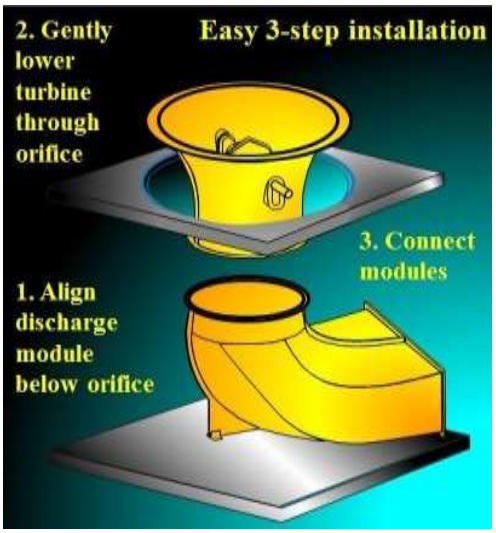

3-Step installation of turbine-generator and discharge modules

Harvester as it would appear following installation

EBID Drop 8 East-side installation *September 24, 2014*

Installation time: ~1Hr

EBID Drop 8 West-side installation *October 22, 2014*

Installation time: <1Hr

Impact: The systems-engineered design enables rapid manufacturing and assembly of desired size units that can be deployed at sites along U.S. waterways as small-hydropower plants. There is worldwide potential for this technology to provide sustainable hydropower to communities isolated from grid-supply.

Ease of Maintenance and Repair

If the repair and maintenance is during irrigation season, steps are needed to block the water entering the drop site. These are operational issues which the irrigation crew know how to perform so that maintenance crew can remove the turbine-generator module from the orifice. Recognizing the rapid deployment capability demonstrated in two prior deployments, the hoisting process can be reversed in the same interval of time to remove the turbine components for replacement or for repair. As easily as the harvester is deployed, the harvester turbine-generator and discharge modules can be decoupled by disconnecting the flanged joints and the turbine-generator module can be hoisted out of the drop site and transported for repair. A replacement unit can then be inserted and coupled to the existing discharge tube making it ready for deployment.

Future Outlook for Small-Hydro

The ability to rapidly transform an existing drop structure in to a small hydropower plant is indeed a revolutionary outcome of the HyPER harvester Project. The manufacturing process that was adopted paves the way for the use of advanced manufacturing techniques wherein strict tolerances can be met during fabrication to produce reliable and highly efficient harvesting units. The Project has clearly demonstrated several key attributes including scalability, modularity, the availability of off-the-shelf electrical and electromechanical components, and the ease of fabricating modular turbine components that allow rapid assembly of harvesters, all contribute towards the feasibility of the HyPER harvester as an efficient *Plug-&-Play* system to harvest hydropower at low-head drops. This significant outcome is illustrated in the graphic below showing the manufacturing of Carbon-composite turbine components to custom-fit an existing drop structure and in transforming the structure into a small hydropower plant. This outcome points to the possibilities for developing low-cost hydropower plants at a multitude of sites here in the U.S., Canada, Mexico and worldwide including parts of Southeast Asia, namely, Vietnam, Laos, Cambodia, Thailand and Myanmar where low-head hydro appears to be the most abundant renewable energy resource. With emphasis on the environment and the ecology, the harvester technology is aesthetic in appearance and has characteristics that are environmentally benign. Furthermore, through advanced impeller design, the possibilities for low-speed impeller motion enables a fish-friendly passage through the turbine.

Adaptability

It is recognized that the EBID Drop 8 Station is unique, and in some instances it may be difficult to integrate the harvester into other existing structures unless some means to channel the flows through the turbine are considered. However, as at Drop 8, we believe the shape and form of the harvester can be engineered to conform to space constraints while maintaining the best flow characteristics through the turbine cavity. The possibilities for optimization of pressure and discharge through the cavity is shown by its scalability. The Kaplan-type design makes the harvester a more desirable technology due to its higher efficiency. This fact enables the application of the HyPER harvester in other types of control structures.

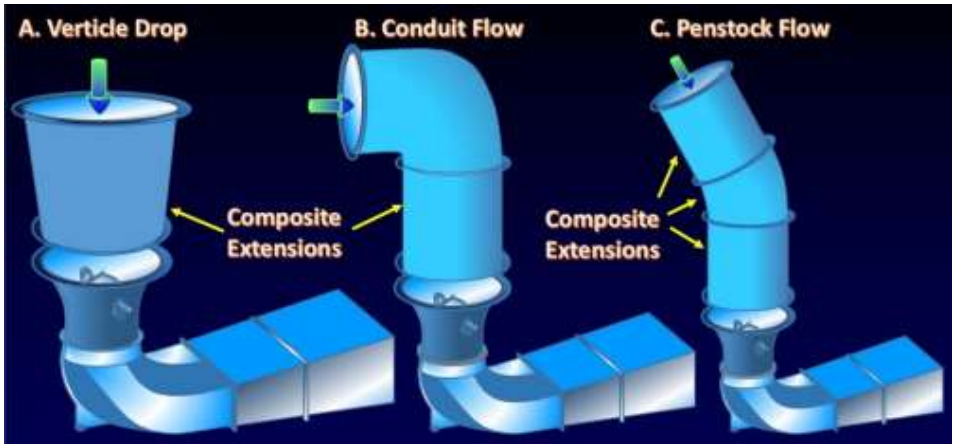

Figure 1. Possible harvester configurations due to drop in elevation

Figure 1 shows various forms of drops in elevation that permit harvester implementation in a conventional hydro configuration. For example, configuration A is similar to Drop 8, but with additional space between orifice and harvester requiring an extension of a truncated conical conduit fabricated using composite materials. This extension can be dropped into the orifice and connected by flange couplings to the harvester below. Configuration B shows a conduit flow drop in which cylindrical conduits (flexible tubes, in their simplest form) could serve as intake to the turbines. Configuration C shows spillway/penstock flow that makes use of conduit extensions to channel flow into the turbines. In all cases, the shape and form of the turbine remains the same, reinforcing the notion of scalability of the turbine-generating system.

Figure 2 shows the turbine-generator module and discharge module that make up a novel low-head 10kW hydropower harvester prototype. Two prototypes were fabricated at MTEC, the manufacturing Center at New Mexico State University. The harvester is scalable and modular with an easy 3-step installation, making it a plug-&-play system. Built entirely of Carbon composite material and fiberglass the harvester is light weight. The modular turbine components make it easy to assemble off-the-shelf electrical and electromechanical components inside a submarine enclosure. Rapid deployment, of less than 1 Hour to install each harvester, clearly establishes a benchmark for developing small hydropower plants.

Figure 2. Shop floor testing of self-supporting structure

The self-supporting attribute makes it unique in that the harvester has minimal impact on the load bearing capacity of existing infrastructure. Scalability allows incremental-sized turbine-generator modular units, for example, 5kW, 10kW, 15kW, 20kW, 25kW, etc., to be easily manufactured using off-the-shelf generating hardware and enclosed inside prefabricated composite material moldings. These attributes enable rapid development of incrementally sized small-hydro and mini-hydro power plants in the U.S., and worldwide.

The hand-crafted modular turbine components establishes a clear basis for the use of advanced additive manufacturing techniques to rapidly manufacture on demand the desired size units for deployment. The manufacturing process begins with the fabrication of turbine and discharge molds that allow multiple castings of the turbine components. The HyPER Harvester Project required the fabrication of two prototypes. Through an additive layering technique of placing alternate layers of Carbon fiber and fiberglass material bonded by epoxy, all turbine components including the Venturi-turbine, discharge elbow, and the submarine are fabricated as half-moldings. The impeller is also fabricated using Carbon-composites. Together, the structural attributes of the harvester are stronger than that of Steel, giving a clear understanding of its durability and ability to withstand the harsh environment of irrigation water.

Technical and other issues pertaining to cost, availability and suitability of generating equipment

Permanent magnet alternators (PMA) are ideally suited for hydropower generation due to low-speed operation and high power output capabilities. Presently, there are only a few manufacturers worldwide who offer low-speed PMAs, but at a very high price of $1.50/Watt, or $15,000 for a 10kW alternator. Additionally, these alternators by virtue of their design characteristics are intended for wind-power generation and with some design modifications are adapted for hydropower applications. In the vertical-axis configuration, as in the HyPER harvester, a suitable thrust bearing is essential to prevent the rotor of the alternator from pulling out due to vertical forces acting on the impeller which is connected directly to the alternator shaft by a coupler. Manufacturers therefore add-on a substantial cost by including a custom-designed thrust bearing so that they can provide the product warranty. Our experience has shown that there is little negotiation possible to lower the cost of generating equipment. This is true, especially with European vendors,

Cost-Model Summary

Present	Future Target
Manufacturing cost $2.93/Watt Radial-flux PM Alternator: $1.32/Watt Instrumentation + Power Electronics $0.45/Watt Turbine, submarine, discharge tube and impeller fabrication $1.16/Watt	**Manufacturing cost < $2.00/Watt** Axial-flux PM Alternator: < $0.80/Watt Instrumentation + Power Electronics < $0.40/Watt Turbine, submarine, discharge tube and impeller fabrication < $0.80/Watt
Fixed Cost Rate: 10% Period: 20 Years Plant Capacity 20kW: 2-10kW Capacity Factor: 75%	Fixed Cost Rate: 10% Period: 20 Years Plant Capacity 20kW: 2-10kW Capacity Factor: 75%
LCOE $0.067/kWh	**LCOE < $0.046/kWh**

Figure 3 below illustrates how a simple modification of the USBR Leasburg check structure using prefabricated structural components, can effectively integrate the harvesters in its present form. This type of 'out-of-the-box' thinking will provide a broad range of applications.

Figure 3. Possibility to transform a check structure into a drop structure

1. Principal Design Criteria

The historic nature of the Drop 8 Station clearly established a principal design criteria that no modifications will be made on the existing structure, satisfying the NEPA criteria. Hence, the harvester had to be made self-supporting thereby eliminating any additional loading on the structure. The harvester had to be modular and light weight so that installation would require a minimum number of crew and equipment and could be done rapidly. The height of the turbine module had to be such that it could slide under the concrete cylindrical gates at its maximum opening before being lowered into the drop orifice. The goal, therefore, was to create a plug & play architecture with minimal intrusion on the existing structure. The Figure 4 illustrates the design characteristics and the possibilities for implementation.

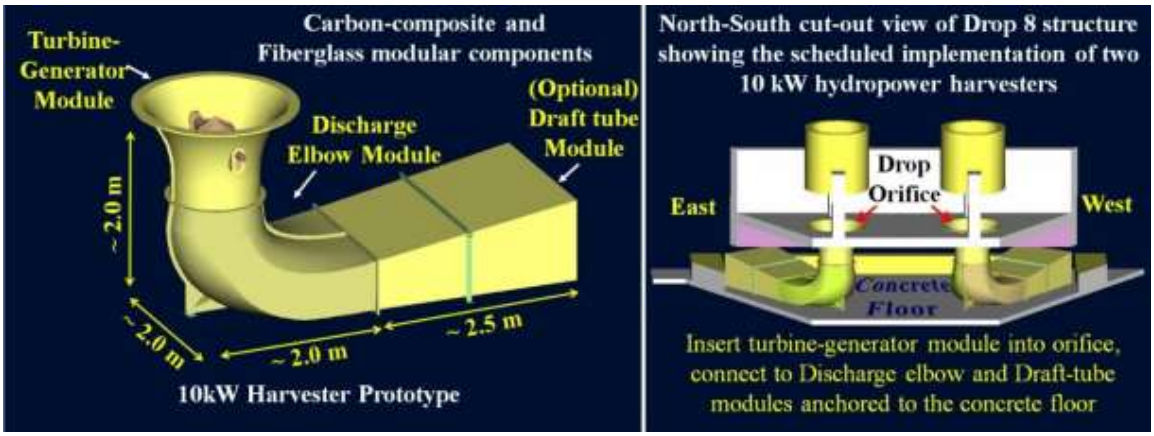

Figure 4, Harvester design and implementation concept

2. Research and Systems Engineering

A 3D model of Drop 8 provided the boundary conditions for computational fluid dynamic simulations. Base-case simulations yielded the maximum flows through the two circular orifices. Based on an effective head of approximately 2 meters and discharge of 3.5 m^3/s, turbine parameters were optimized for maximum flow conditions. Figure 5 shows the 3D model of Drop 8 and a 3D fluid dynamic simulation showing the velocity at maximum discharge. (See Appendix for detailed design)

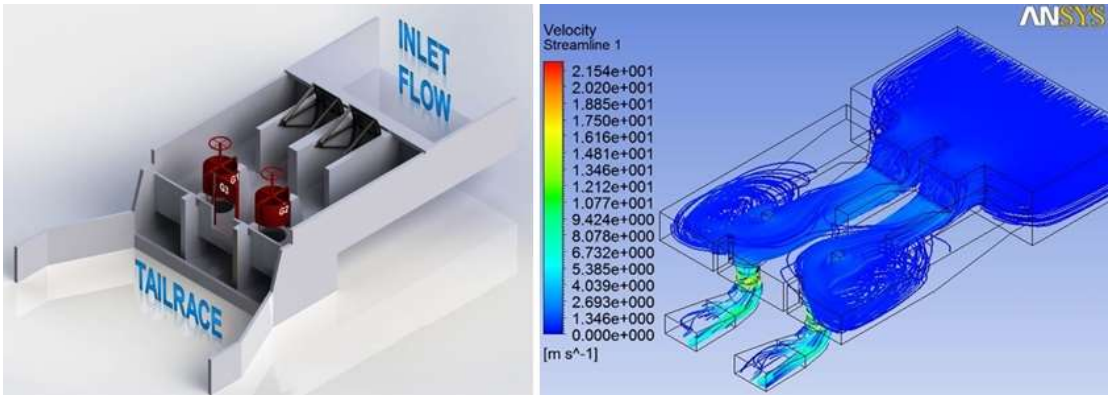

Figure 5. 3D Model of Drop 8 and CFD simulation at maximum flow conditions

3. Fabrication: *From molds to modular turbine elements*

A brief video shows the turbine assembly highlighting modularity. The following Tables provide a cost summary for fabricating one and two 10kW prototypes.

Table 1. Cost of materials to fabricate harvesters expressed in $/Watt

Materials cost (Carbon-composites, Resins and all associated materials)	
One-time mold material cost	$1,400
Recurring material cost per 10kW harvester	$2,450
Materials Cost for 1-10kW harvester = ($1,400+$2,450) = $3,850	
Materials Cost for 2-10kW harvesters = ($1,400+2{$2,450}) = $6,300	
Average Materials cost per Harvester = ($3,850+$6,300)/2 = $5,075	
Materials Cost/Watt for 1-10kW Harvester = $3,850/10kW = $0.39/Watt	
Materials Cost/Watt for 2-10kW Harvesters = $5,075/20kW = $0.25/Watt	

Table 2. Cost of fabricating turbine components expressed in $/Watt

Mold fabrication, composite turbine castings and assembly costs		
Task Description	Current Cost	Targeted Cost with Advanced Manufacturing
Mold Fabrication (M)	$5,920	$4,250
Turbine Castings (T)	$4,850	$2,250
Harvester Assembly (H)	$1,500	$1,500
Cost of 1st 10kW Harvester=(M)+(T)+(H)=$12,270 Cost of 2nd 10kW Harvester=[(T)+(H)]=$6,350 Average Cost per 10kW harvester=$9,310 Cost of Manufacturing=$9,310/10kW = $0.93/Watt		Cost of 1st 10kW Harvester=(M)+(T)+(H)=$8,000 Cost of 2nd 10kW Harvester=[(T)+(H)]=$3,750 Average Cost per 10kW harvester=$5,875 Cost of Manufacturing=$5,875/10kW = ~ $0.60/Watt

Table 3. Cost of harvesters with Radial-Flux Alternator expressed in $/Watt

Manufacturing cost for one, and two 10kW harvesters with Radial-Flux PMA							
Number of Units fabricated	Mold Materials & Mold Fab.(Labor)	Carbon-composites & Materials	Composite Castings (Labor)	PMA & Pwr. Elec.	Assembly Labor	Total Fab. Cost	$/Watt
1st Unit	$5,920	$2,450	$4,850	$17,500	$1,500	$32,220	$3.222/W
2nd Unit	$0	$2,450	$4,850	$17,500	$1,500	$26,300	$2.630/W
Average Cost per 10kW harvester with Radial-Flux PMA						$29,260	$2.93/W

It is clear from Tables 1-3, that the cost of fabricating two or more harvesters has the strong potential for reducing the cost of manufacturing significantly. Presently, the cost of manufacturing stands at $2.93/Watt with the cost of power generating components at nearly $1.80/Watt. With current manufacturing cost remaining the same, the use of axial-flux PMAs, however, reduces the overall cost to $2.20/Watt as illustrated in Table 4.

Table 4. Cost of harvesters with Axial-Flux Alternator expressed in $/Watt

Manufacturing cost for one, and two 10kW harvesters with Axial-Flux PMA							
Number of Units fabricated	Mold Materials & Mold Fab. (Labor)	Carbon-composites & Materials	Composite Castings Labor	PMA & Pwr. Elec.	Assembly Labor	Total Fab. Cost	$/Watt
1st Unit	$5,920	$2,450	$4,850	$10,200	$1,500	$24,920	$2.49/W
2nd Unit	$0	$2,450	$5,850	$10,200	$1,500	$19,000	$1.90/W
Average Cost per 10kW harvester with Axial-Flux PMA						$21,960	$2.20/W

Table 5. Cost of harvesters with Axial-Flux Alternator expressed in $/Watt

Advanced Manufacturing cost with Axial-Flux PMA							
Number of Units fabricated	Mold Materials & Mold Fab. (Labor)	Carbon-composites & Materials	Composite Castings Labor	PMA & Pwr. Elec.	Assembly Labor	Total Fab. Cost	$/Watt
1st Unit	$4,250	$2,450	$2,250	$10,200	$1,500	$20,650	$2.07/W
2nd Unit	$0	$2,450	$2,250	$10,200	$1,500	$16,400	$1.64/W
Average Cost per 10kW harvester with Axial-Flux PMA						$18,525	$1.85/W

From Table 5 it is seen that advanced manufacturing can significantly lower the cost of fabricating turbine components to approximately $1.85/Watt.

Figure 6 shows mold shapes for the turbine, discharge elbow and submarine and the number of molds required for fabricating castings.

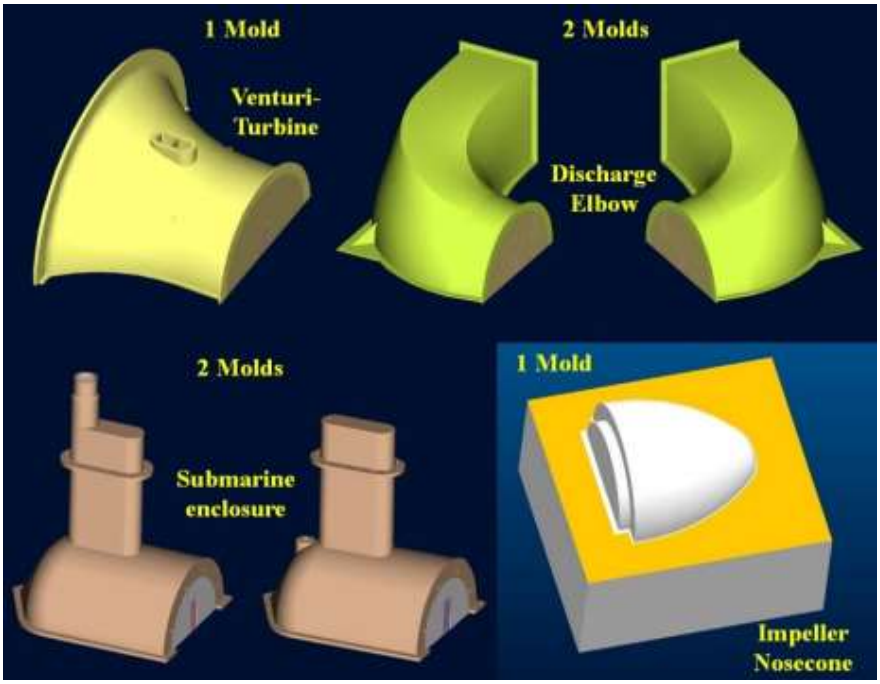

Figure 6. Mold shapes and the number of molds required to fabricate multiple turbine castings

Figure 7. Molds in various stages of fabrication.

4. Deployment: *From Factory-to-Field*

Figure 8. 1) Turbine modules ready for installation at the Drop 8 Station; 2) Hoisting the discharge module; 3) Placing the discharge module under the drop orifice; 4) Bracing the turbine; 5) Hoisting the turbine; 6) Placing the turbine above orifice

Figure 9a. EBID Drop 8 East-side installation *September 24, 2014*

Figure 9b. EBID Drop 8 West-side installation *October 22, 2014*.

5. Test and Evaluation

First set of tests

Water was released into the EBID irrigation canals on May 28th, 2015. Flows show the normal early irrigation season flowrate of about 8.5 m^3/s, approx. 300 cfs. While the cylindrical gate covering the Eastside turbine remained "closed", there was still a substantial amount of water being discharged through the turbine. As such, the East-side harvester at Drop 8 Station began to operate immediately following water release. With the unit having been in service for over a week, on June 6, 2015, a limited-scale test was conducted by opening the cylindrical gate to its full extension and allowing normal flow through the turbine, approximately 3.5 m^3/s. As expected, some structural vibration was experienced due to imbalance in the impeller. The composite impeller could not be spin-tested in the MTEC machine shop prior to its implementation. With gate in full open position and after about 2 hours of operation, the impeller assembly comprising the thrust bearing, shaft and impeller unexpectedly pulled out of the turbine and due to its light weight floated downstream. This failure-mode was not anticipated.

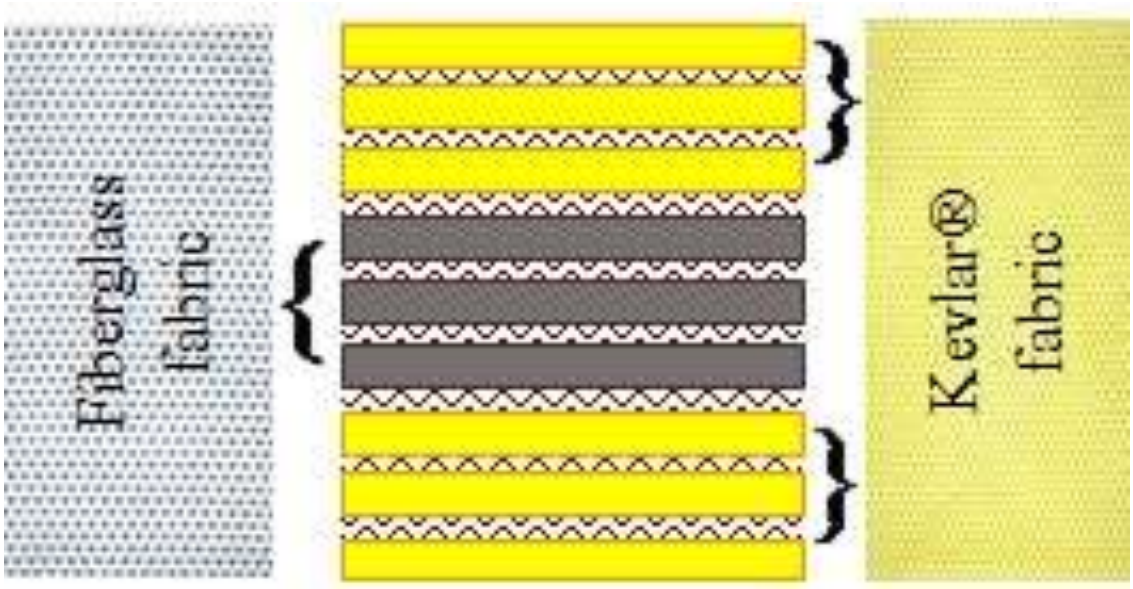

Figure 10. Layers of Kevlar® and Fiberglass bonded in epoxy

Figure 10 illustrates a cross-section of the layers comprising the (1/2)" wall thickness of the submarine and venturi-turbine castings. The (1/2)" wall thickness of the Carbon-composite submarine shell has a minimum yield strength of **36,000 psi** (**250 MPa**) and ultimate tensile strength of **70,000–80,000 psi**. This is based on tensile tests of samples taken from moldings during fabrication.

After retrieving the assembly from downstream, an inspection of the impeller assembly indicated no damage to the thrust bearing or to any portion of the assembly. Because the turbine could not be removed for inspection due to its inline implementation, we surmise the composite material

that held the assembly in place may have frayed, i.e., the layers of composite material separated along the edge of the submarine giving way for the assembly to be pulled out.

Figures 11a and 11b show the shaft coupling and thrust bearing assembly inside the harvester submarine, and the possible failure point in the submarine end-plate from which the impeller appears to have pulled out. This was confirmed after removing the turbine from Drop 8.

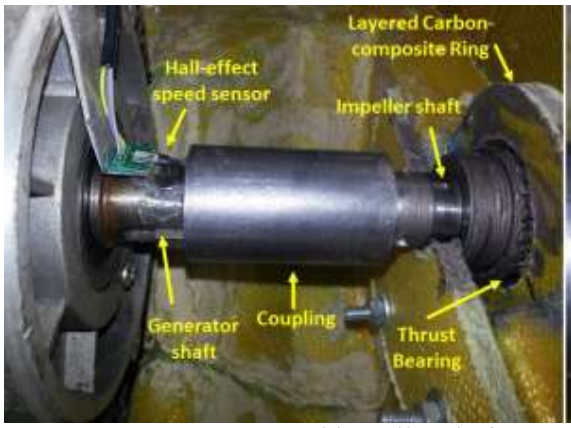

Figure 11a. Generator and impeller shaft coupling

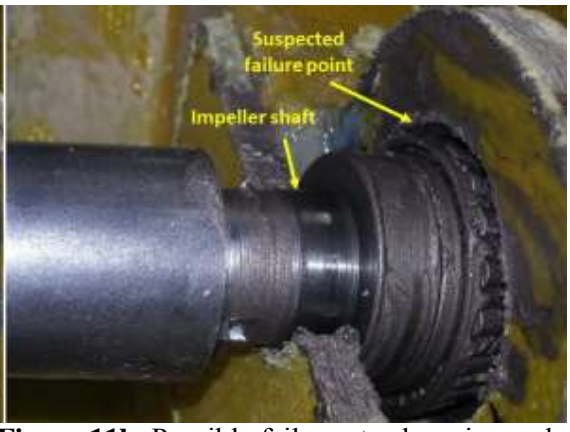

Figure 11b. Possible failure at submarine end-plate

Figure 12. Modification to the end-plate design. The new endplate is made of Stainless Steel to support the impeller weight plus the active axial-thrust during water flow. Manufacturer of impeller guarantees the endplate withstand capability is 10,500 lbs which is about 1.6 times larger than the estimated axial thrust of 6,500 lbs.

On May 22, 2015, one week prior to water release on May 28, 2015, the West-side unit was removed from Drop 8 Station for the purpose of replacing the Carbon-composite impeller by a new Aluminum impeller fabricated as part of the EBID cost sharing agreement. Figure 13a shows the Aluminum impeller and Figure 13b shows the Carbon-composite impeller that pulled out from the Eastside Unit.

Figure 13a. 30^0 blade angle, 4-blade Aluminum impeller

Figure 13b. Carbon composite impeller assembly

Figure 14 shows the composite impeller replaced by the Aluminum impeller, and other minor design changes that assure greater operating reliability.

Figure 14. West-side unit with Aluminum impeller

Second set of tests

Water was released into the EBID irrigation canal on October 8th, 2015. The inlet remained "closed" until sufficient pressure head was developed to conduct tests. Based on the inlet pressure head and gate opening, flowrate of about 4.0 m^3/s, approx. 140 cfs was observed. As evidenced in the following video, substantial amount of floating debris can be seen flowing through Drop 8. Although efforts were made to remove the debris upstream using a large mechanical hoe, the passage of smaller debris could not be avoided.

Figure 15. Inlet gates to Drop 8 closed for water level to buildup to maximum level

The test setup included a 20 Ohm resistor load bank and five 500 Watt incandescent lamps, a laptop computer with LabView® software to collect alternator speed, voltage, load current, pressure drop across the impeller and mechanical vibration. As the gates were opened to allow water for testing one of the crew members accidentally pulled on the USB cable connecting the electronics and all data transmission from the instrumentation package ceased. Approximately five minutes of data was recorded. A backup plan was immediately initiated to record the voltage and frequency using a Fluke multimeter. This, at a minimum provided output voltage and the frequency from which the speed of the impeller could be calculated. As water filled up the turbine, the alternator voltage and frequency were recorded. Figure 16 summarizes the recorded data. The speed of rotation (RPM) is calculated based on the observed frequencies in Hz.

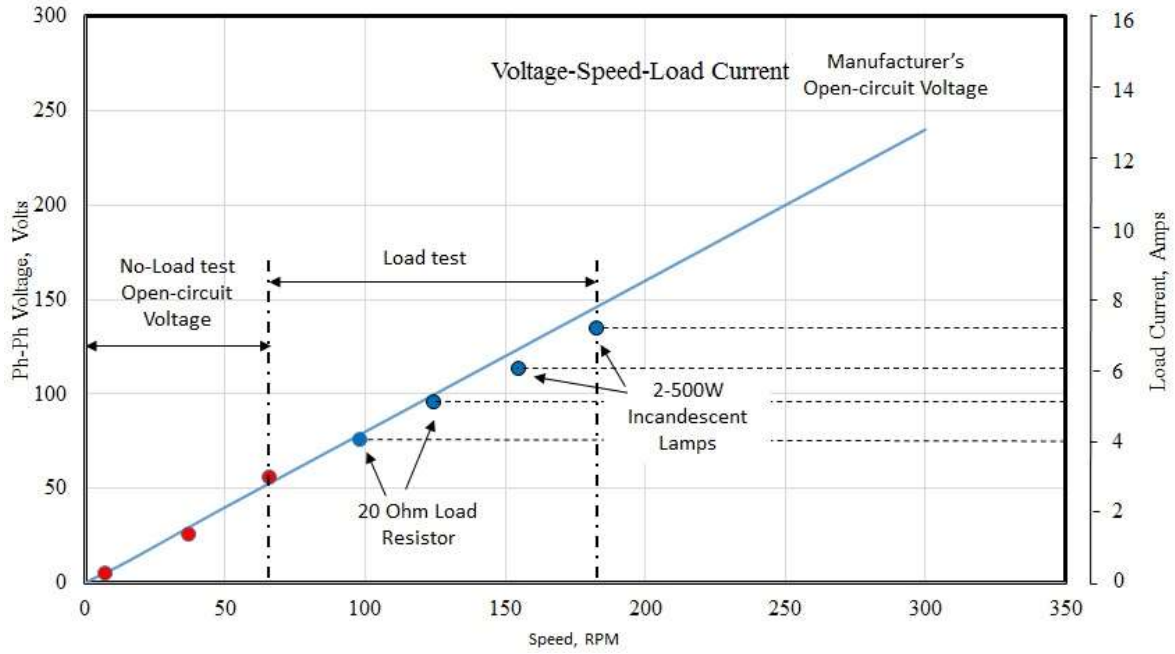

Figure 16. Recorded data

The 3-phase permanent magnet alternator, designed to produce 0.8 Volts phase-phase/RPM, has a rated voltage of 240 Volts at 300 RPM. In one test, measurements were taken using a Fluke multimeter to show variations in voltage and frequency under load as the gate is opened and closed. Opening the gate allowed more water into the turbine causing impeller speed to increase and hence generate higher voltage. Closing the gate allowed less water into the turbine causing the impeller speed to decrease and produce lower voltage. These operations were conducted with the 20 Ohm resistor and two 500 Watt incandescent lamps connected in parallel. The following video shows measurements of the AC RMS phase-phase voltage and the average frequency.

As seen in the video earlier, trash entering the turbine accumulated quite rapidly causing the impeller to stop. The multimeter read 0V AC. Several attempts made to release the trash were unsuccessful. Pictures taken the following day when all water had drained from the drop show small pieces of tumbleweed tightly matted and a piece of wood that caused the impeller to stop.

Figure 17. Debris clogging the turbine

6. Lessons learned

The impeller pullout and difficulties in replacing the impeller onsite suggest that prototype testing, in general, should be carried out in a laboratory wherein controlled tests can be performed reliably thereby mitigating any risks posed by drought and other conditions that prevent inline testing in irrigation canals. Real-world testing is not practical considering time-scheduling with water release and other obligations which the irrigation district may have that would prevent inline testing, and hamper the repair and replacement of components in a timely manner.

The USB pullout during the second set of tests suggests better access to embedded instrumentation.

Varying levels of tailrace suggest improvement in design to eliminate axial vibrations due to hydrodynamic pressure.

Preventing debris from entering the turbine remains a major concern in irrigation canals.

APPENDIX

Harvester Design

1. Design Overview

The design considers recent and historical flow characteristics at the Drop 8 structure as a means to estimate the site power generating capacity. Based on the physical geometry of the structure, CFD simulations provide estimates of the harvesting potential. Based on average flow conditions, the design guarantees over 20 kW of generation at the Drop 8 site.

1.1. Elephant Butte Irrigation District (EBID) Drop 8 structure

Built in the 1990's, the EBID Drop 8 structure has served to prevent soil erosion at the natural drop site, while simultaneously providing the means to control irrigation water to farming communities along the canal. The engineering task then was primarily to build a concrete structure so as to distribute the natural flow-pattern through a pair of inlet gates and a set of three drops, while maintaining continuous flow. Wheel-operated gates provided the capability to block or reduce water passing through any drop.

EBID Drop 8


Gated Outlet


Gated Inlet

The historic nature of the Drop 8 structure poses itself as the fundamental constraint in the design and development of the hydropower harvester. With the present goal to harvest energy at Drop 8, there is a strong desire to preserve the physical structure in the original form without any civil-engineering modifications. The goal then is to design a self-supporting harvester that can be scaled to fit within the constraints with a plug-and-play modular architecture. Meeting such a goal will show scalability over a range of hydropower generation from drop structures throughout the U.S.

Pictures below illustrate the drop structure in the dry season from around October through May. a) Inlet flow divides into two flow paths. b) Inside the reservoir water drops through two circular orifices D1 and D2. c) Flow D3 occurs through the gate at the outlet of the Drop 8 structure.


a) Inlet flow pattern

b) Reservoir flow pattern

c) Outlet flow pattern

(Pictures taken in November 2011, Dry season Oct. - May)

Pictures below show flows through the drop structure during the irrigation season which lasts from around June through September. Picture on left shows flow conditions through the inlet are about 40-50% of the maximum flow (roughly 1 meter (3 ft.) head). Water entering the inlet is regulated by arc-shaped gates. Center picture shows the reservoir with two drops. As water enters the reservoir, flow splits between the drops and the gated outlet. Right picture shows flow through the outlet gate G3 of the drop structure. Gate G3 is manually controllable. Flow-control gates offer the possibility for maximizing hydropower generation at this historic irrigation structure.

d) Inlet Flow

e) Reservoir Flow

Outlet Flow

(Pictures were taken in July 2012, Irrigation season)

2012-13 Dry season watermarks: Pictures taken in January 2013 illustrate many historical flow characteristics at the drop structure. Closeup view the inlet shows watermarks from decades of flow. From this information, we can get a relatively strong perception of the inlet flows that may be expected during a bountiful irrigation season. From the maximum height, it is easy to estimate the maximum head available at the inlet to Drop 8 as roughly 6 ft (1.83m).

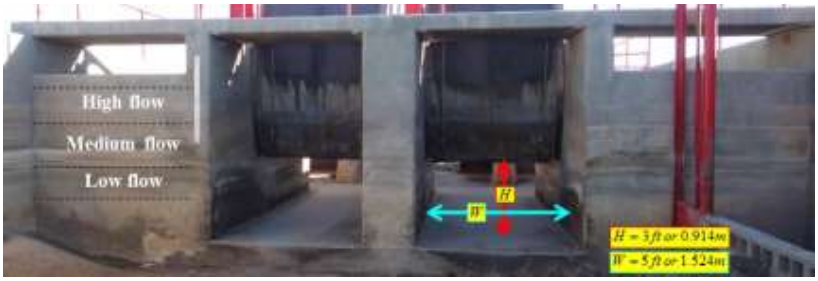

Watermark bands on the concrete wall and on the steel gates graphically illustrate the inlet flow characteristics and are marked appropriately as High, Medium and Low flows

Watermarks of the plume formed at the inlet shows the crest line is approximately 4 feet above the reservoir base.

Watermarks inside the reservoir confirm the maximum head and provide boundary conditions for CFD studies.

1.2. Drop 8 3D Model

A 3D model of the Drop 8 structure in Figure 3 illustrates flow paths corresponding to the inlet, the two drops D1 and D2, and outlet flow D3 through gate 3. Outlet flow G3 can be controlled so as to maintain a constant head in the reservoir. For example, during high flow conditions with 500 CFS flow through the inlet and with gate G3 fully closed, it is likely that the reservoir will overflow. Overflow can be avoided by keeping gate G3 partially open to allow excess water to flow through the gate. Although all gates can be controlled, operability is presently restricted to manual operation of Gate G3.

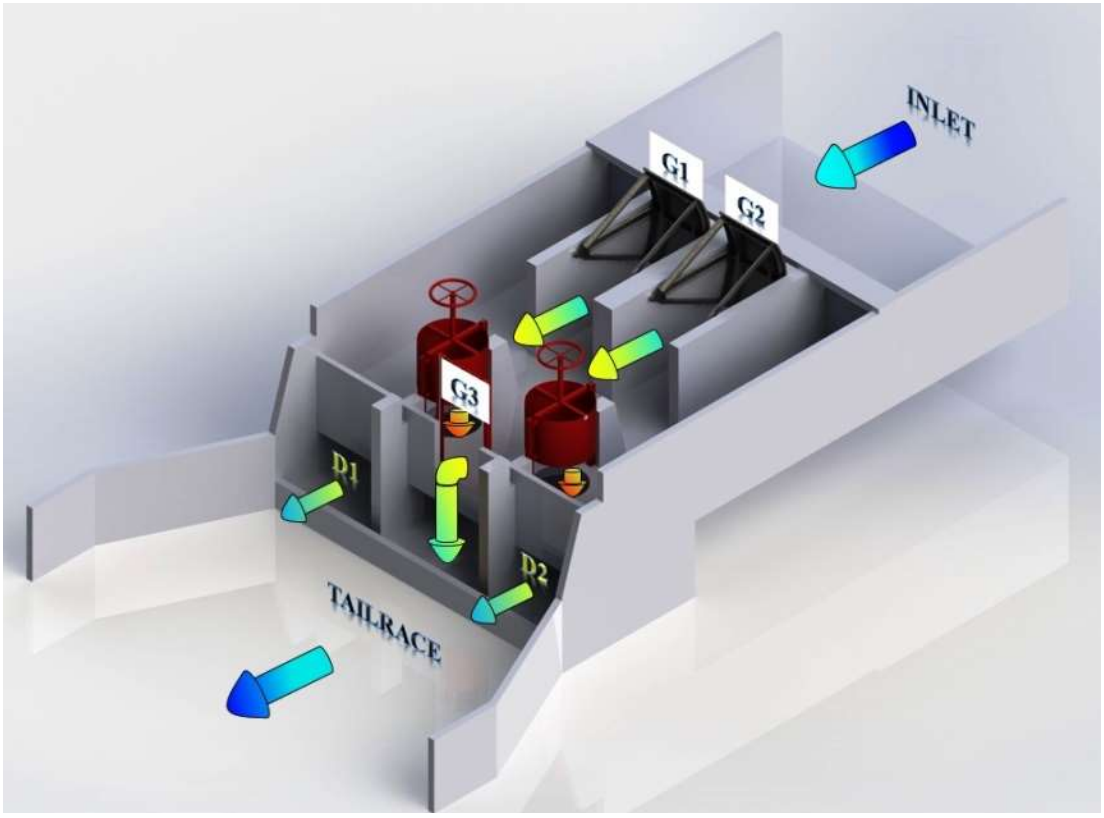

Figure 3. 3D model of Drop 8 structure for fluid dynamic boundary conditions

To better understand the amount of hydropower that can be harvested, it is necessary to determine the distribution of the inlet water between the two drops D1 and D2 with the outlet through Gate G3 blocked.

Referring to Figure 3, we observe that closing Gate 3 causes the reservoir to fill up until the maximum head is reached and water from the reservoir begins to overflow. With the outlet blocked, the head inside the reservoir stabilizes when total discharge through the drops is equal to the inlet. Maximum discharge through drops D1 and D2 occur at maximum head of 4 ft or 1.22 m in the reservoir.

1.3. Calculation of maximum discharge through drops D1 and D2

Maximum head above each drop is 48" or 1.2192m (this is the wall height of the reservoir)

> Note: Head directly above a orifice (reservoir height above the drops) is determined by the cusp of the water level caused by a vortex. The effective head, therefore, is less than that prescribed by the wall height of the reservoir. Ignoring this drop in height due to the vortex yields the ideal head. At this head, the water surface is flat.

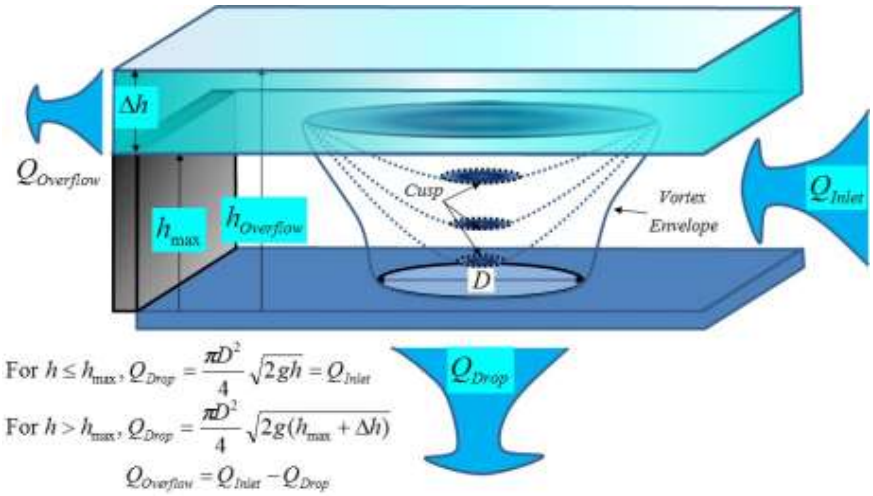

Ideal velocity at the drop inlet

$V_{ideal} = \sqrt{2gh} = \sqrt{2*9.81*1.2192} = 4.8909\, m/\sec or\ 16.0463\, ft/\sec$

The diameter *D* of each drop is 52" or 1.3208m (radius = 26" or 0.6604m)

Ideal discharge through each drop

$Q_{ideal} = AV_{ideal} = \pi(0.6604)^2(4.8909) = 6.7012\, m^3/\sec or\ 236.6506\, ft^3/\sec$

At maximum reservoir head, output through the drops is at a maximum. The total ideal discharge through the two drops is, therefore, 13.4024 m^3/sec or 473.3012 ft^3/sec.

Actual discharge through an orifice is less than the ideal discharge due to losses caused by friction. To account for this loss, the coefficient of discharge is computed as a product of the coefficient of velocity and a coefficient of contraction. Coefficient of velocity C_v, is the ratio of actual velocity to the ideal velocity. The coefficient of contraction C_c, comes into effect as a result of non-rectangular cross-section at the inlet of an orifice. C_c is the ratio of the area of cross-section at the orifice inlet to area of cross-section when the flow has become constant at *vena contracta*. It is noted that as pressure head increases the cross-sectional area at vena contracta increases, thereby increasing the orifice discharge at higher velocity.

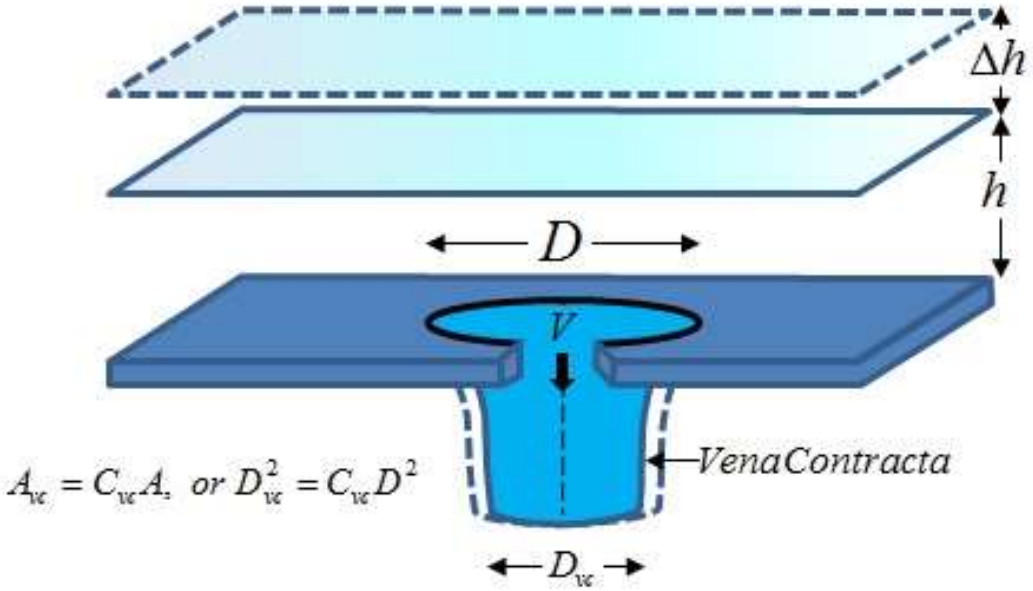

From the figure above, it is seen the actual discharge would be reduced by an amount proportional to the reduction in cross-sectional area of the water column due to contraction. Hence,

$$Q_{actual} = C_{vc}A_{vc}V_{vc} = C_V C_c AV = C_D Q_{ideal}$$

The coefficient of discharge for circular orifices is typically in range 0.6 – 0.9. Therefore, the possible range of discharge is computed as:

$$Q_{0.6} = 0.6 \times 6.7012 \cong 4.02 m^3/s \ \ per\ drop;\ Q_{0.9} = 0.9 \times 6.7012 \cong 6.03 m^3/s \ \ per\ drop$$

A benchmark for CFD simulations is the range of discharge between $4 m^3/s$ to $6 m^3/s$. The best estimate for the coefficient of discharge is actually obtained from the mass-flow rates determined by CFD simulations in relation to the ideal discharge of $6.7012 m^3/\text{sec}\ per\ drop$ or $236.6506\ ft^3/\text{sec}\ per\ drop$.

With the boundary conditions established for three flow patterns, Figure 4 illustrates basecase CFD simulations of fluid flow through the gate structure during high, medium and low-flow conditions and shows the following distribution of water through the 3 gates.

From the distribution of flows through the Drop 8 structure, it is evident during high-flow conditions that the flow through each drop is approximately $4.81 m^3/s$. As such the coefficient of discharge may be computed as follows:

$$Q_{actual} = C_C C_V A\sqrt{2gh} = C_D A\sqrt{2gh} = C_D \pi \frac{D^2}{4}\sqrt{2gh} = C_D Q_{Ideal}$$

Where,

$C_C = Coefficient\ of\ contraction$ $A = Cross-sectional\ area\ of\ the\ orifice$

$C_V = Coefficient\ of\ velocity$ $h = height\ of\ water\ above\ the\ orifice$

$C_D = C_C C_V = Coefficient\ of\ discharge$ $g = acceleration\ due\ to\ gravity\ constan$

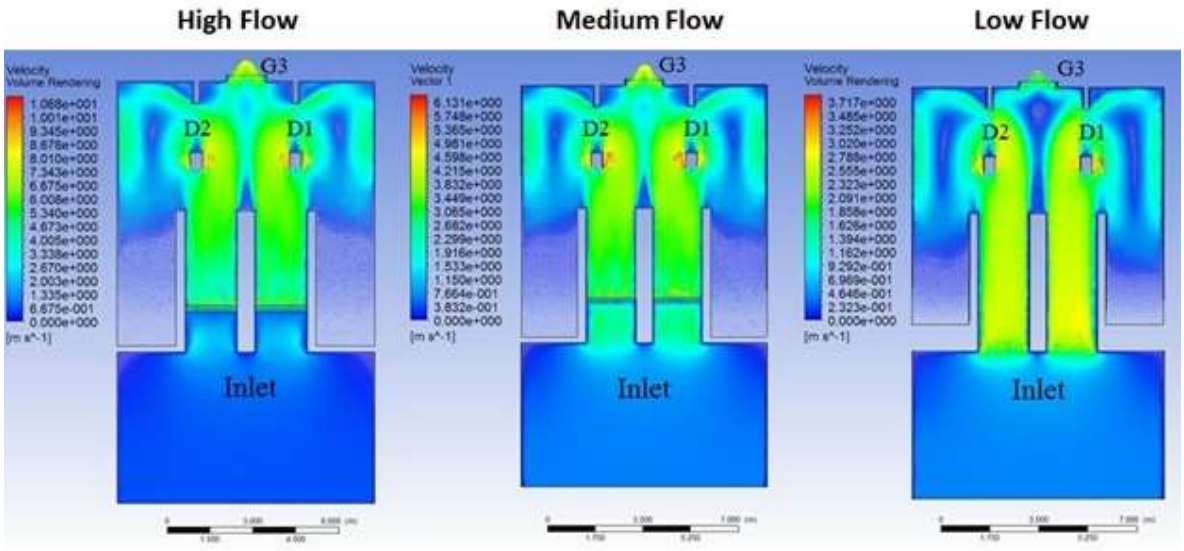

Inlet Flow
$14.12 m^3/s$ *or* 500 ft^3/s

Inlet Flow
$8.48 m^3/s$ *or* 370 ft^3/s

Inlet Flow
$3.27 m^3/s$ *or* 115 ft^3/s

Mass Flow Rate	(Kg/s)	Mass Flow Rate	(Kg/s)	Mass Flow Rate	(Kg/s)
Inlet	14154.445	**Inlet**	8478.991	**Inlet**	3270.7936
Drop D1	-4805.8132	**Drop D1**	-2839.3139	**Drop D1**	-1290.7352
Drop D2	-4809.3891	**Drop D2**	-2848.1885	**Drop D2**	-1233.2092
Gate G3	-4539.6791	**Gate G3**	-2791.6943	**Gate G3**	-747.01008
Net	-0.43673071	**Net**	-0.20564578	**Net**	-0.1609182

Figure 4. CFD simulations of three typical flow rates at Drop 8

Therefore, $C_D = \dfrac{Q_{Actual}}{Q_{Ideal}} = \dfrac{4.81}{6.03} \approx 0.8$

From the Table of mass-flow rates in Figure 4, it is observed that during high-flow and medium-flow conditions, the distribution of water between the three flow paths is approximately one-third of the total inlet flow. That is, the flows through D1, D2 and G3, each have nearly equal mass-flow rates. However, during low-flow conditions, 77% of the inlet flow drops through D1 and D2 with roughly 22% flowing through G3. This observation suggests that gate G3 can be effectively used to regulate the pressure-head inside the reservoir so that the harvester output can be maximized over a wider time range during the irrigation season. The duration of rated power output can be maximized with Gate 3 control. Although manually controlled at present, this can be automated in the future to vastly improve plant efficiency.

Minimum Capacity of Drop 8

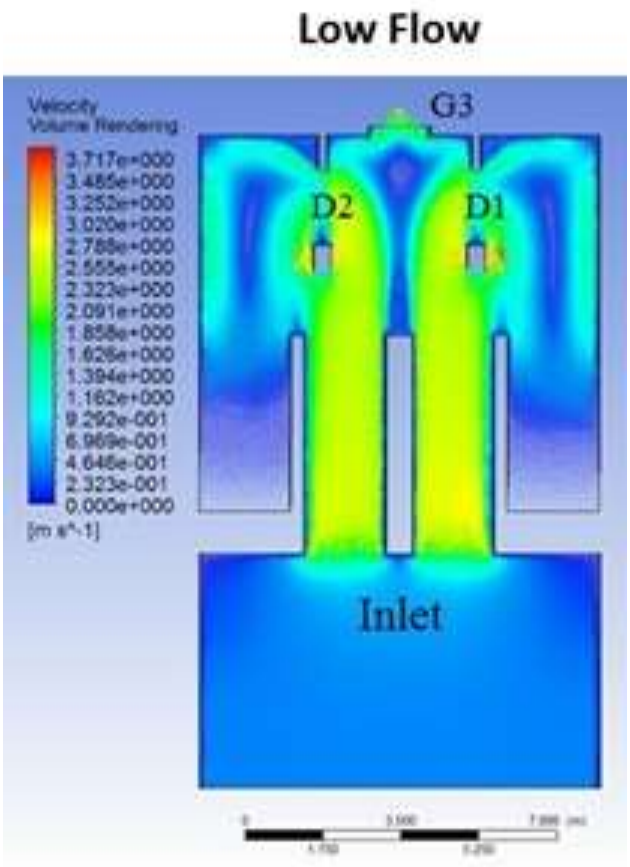

The low-flow basecase provides a baseline for the minimum amount of harvestable power at Drop 8. This estimate is essential in determining the plant cost-to-benefit ratio which has influence in lowering the LCOE. Figure on the left shows the basecase flows through Drop 8 during low-flow rates.

With $3.27 m^3/s$ *or* $115\ ft^3/s$ inlet flow, the average flow through each drop D1 and D2 is nearly $1.26 m^3/s$ *or* $44.5\ ft^3/s$. The drop inlet velocity is approximately $3 m/s$ *or* $9.843\ ft/s$. With outlet G3 flow held at a constant rate of $0.75 m^3/s$ or $26.5\ ft^3/s$, the net head in the reservoir is typically $0.5m$ *or* $1.64 ft$.

By closing gate 3, $0.75 m^3/s$ *or* $26.5\ ft^3/s$ flow can be diverted to increase the amount of flow through each drop. During low-flow periods, therefore, with gate 3 closed all the water entering the Drop 8 structure can be utilized for power generation.

The mass-flow rate $\dot{M} = \rho Q$, where $\rho \approx 1000 kg/m^3$ is the density of water.

For a discharge $Q = 1.64\ m^3/\text{sec}$ through each drop, with an effective head $h \approx 0.5m$ and an efficiency $\eta = 0.8$, the available power from each drop can be computed as:

$$P_e = \eta \dot{M}\ g\ h = 0.8 * 1{,}640.0 * 9.81 * 0.5 = 6{,}435\ Joules/\text{sec}\ or\ 6.435 kW$$

Maximum capacity of Drop 8

During high-flow conditions, for example, at $14.12 m^3/s$ or $500\ ft^3/s$ inlet flowrate, it can be perceived that with gate G3 completely closed the reservoir will overflow. As such by partially closing gate G3, natural flow can be established through the drops D1, D2 and flow through through gate G3. This would allow a constant maximum pressure head to be maintained in the reservoir.

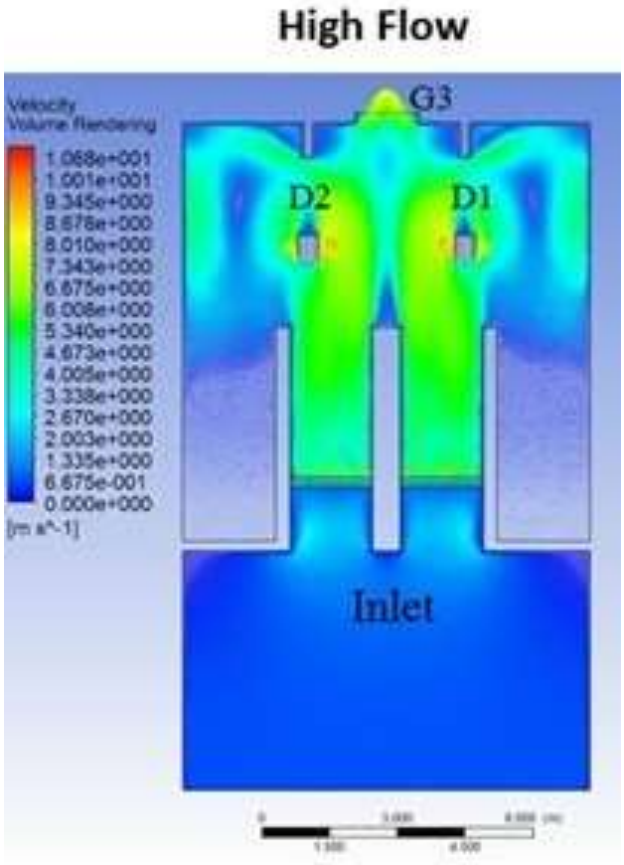

Figure on left shows results from the high-flow basecase with Gate 3 open. The maximum flow through each drop is $\approx 4.8 m^3/s \; or \; 169.5 \; ft^3/s$. The velocity at the inlet of each drop is about $9 m/s$ or $29.53 \; ft/s$. At this flow rate, the water level inside the Drop 8 reservoir is typically $0.91 m \; or \; 3 ft$. With h of $0.91 m$ and an efficiency $\eta = 0.8$, the available power from each drop can be computed as:

$$P_e = \eta \dot{M} \; g \; h$$
$$= 0.8 * 4800.0 * 9.81 * 0.91$$
$$= 34{,}280 \; Joules/\sec \; or \; 34.28 \; kW$$

Now, by partially closing Gate G3 the head in the reservoir can be raised to the maximum, beyond which overflow occurs. The maximum height of the reservoir wall is $1.22 \; m \; or \; 4 ft$. With an effective head h of $1.22 m$ and an efficiency $\eta = 0.8$, the available power from each drop can be computed as:

$$P_e = \eta \dot{M} \; g \; h$$
$$= 0.8 * 4{,}800.0 * 9.81 * 1.22$$
$$= 45{,}958 \; Joules/\sec \; or \approx 46 \; kW$$

The increase in reservoir pressure head as a result of Gate 3 control, combined with the additional flow that can be forced through drops D1 and D2, add credibility to Gate 3 as a key generation control parameter at Drop 8.

Gate G3 Closed

CFD simulations for the high-, medium- and low-flow cases confirm that the reservoir can be maintained at the maximum head for reasonable periods of time during an the irrigation season. With gate G3 closed, the flow which would otherwise drop through G3 can be redirected to maximize the drop discharge through D1 and D2. Hence the Drop 8 plant output can be maximized. Notice in the simulations that the flows for the high-flow case were adjusted so there is no overflow and hence all the water entering the inlet flows through the drops D1 and D2.

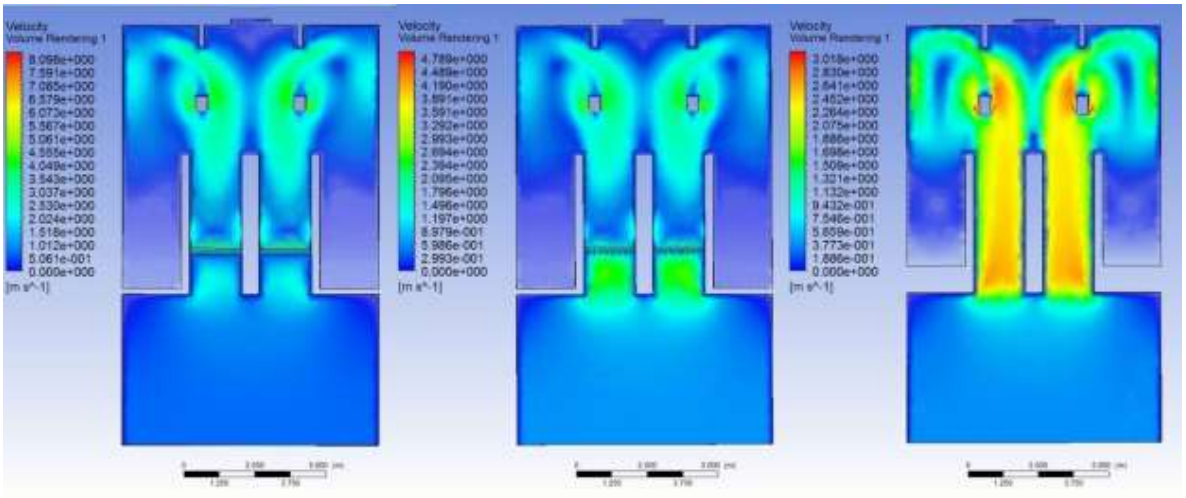

Inlet Flow $9.83 m^3/s$ or $347.14\ ft^3/s$		Inlet Flow $8.48 m^3/s$ or $300\ ft^3/s$		Inlet Flow $3.27 m^3/s$ or $115\ ft^3/s$	
Mass Flow Rate	**(Kg/s)**	**Mass Flow Rate**	**(Kg/s)**	**Mass Flow Rate**	**(Kg/s)**
Inlet	9830.0000	**Inlet**	8480.0000	**Inlet**	3270.7936
Drop D1	-4915.2714	**Drop D1**	-4241.2229	**Drop D1**	-1633.6166
Drop D2	-4913.3131	**Drop D2**	-4239.1325	**Drop D2**	-1633..1062
Gate G3	0.0	**Gate G3**	0.0	**Gate G3**	0.0
Net	-0.5566791	**Net**	-0.35564578	**Net**	-0.1609182

The results confirm the maximum discharge through each drop is approximately $4.91 m^3/s$ $or\ 174\ ft^3/s$. (Caution: Velocity profiles are illustrated in different color scales)

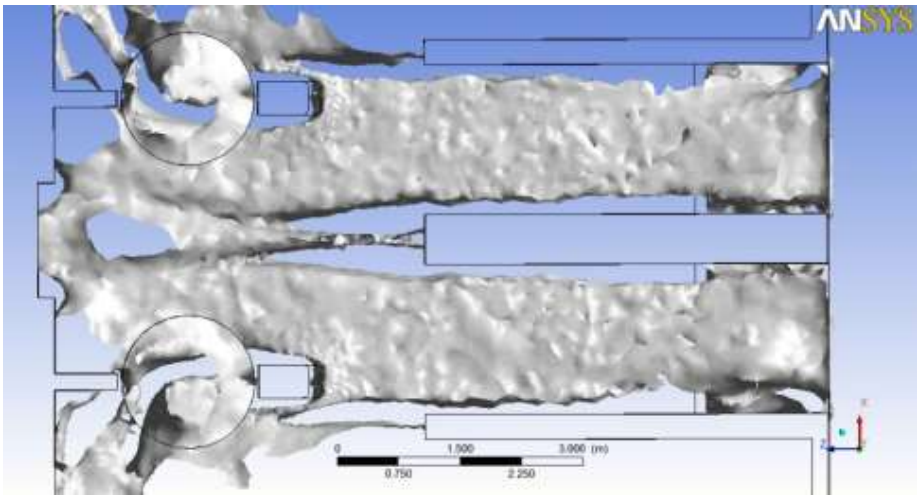

Floor view inside reservoir shows swirls through the drops D1 and D2 in opposite directions

1.4. Reservoir overflow

It is necessary to examine the overflow condition caused by closing Gate G3 to understand the maximum flow condition at the two drops. Overflow occurs when the reservoir is full and discharge through the drops is at a maximum. At maximum flow, the net discharge through the drops is less than the inlet flow. Pressure head rises in the reservoir and there is a tendency for flow through the drops to increase. Since the overflow boundary is unconstrained, excess water will overflow the reservoir wall with only a marginal increase in flow through the drops.

A CFD simulation illustrated in Figure 5 shows reservoir overflow with inlet flow at $15 m^3/s$ *or* $530\ ft^3/s$ with Gate 3 closed. In this case, the net discharge through each drop is approximately $4.9 m^3/s$ *or* $173\ ft^3/s$, a slight increase over the basecase flow of $4.81 m^3/s$. This is indeed the maximum discharge attainable at Drop 8.

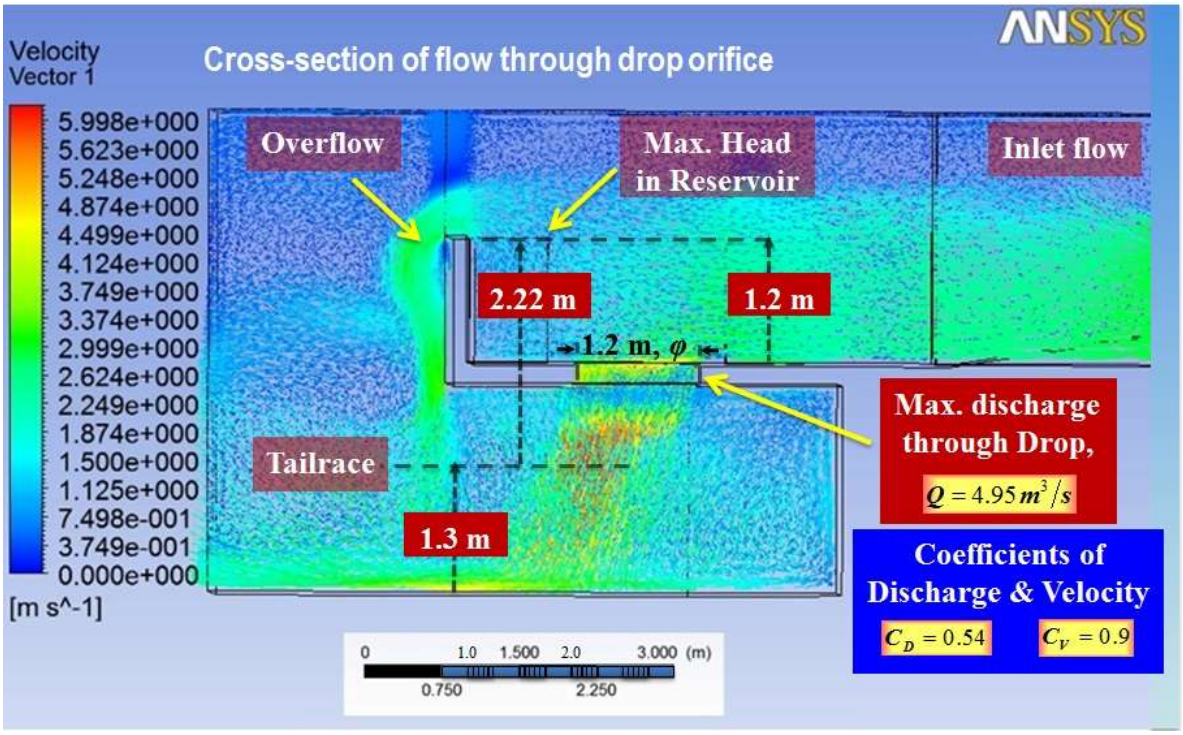

Figure 5. Simulation of overflow condition

Flow regulation would lessen the possibility of cyclic loads on the historic structure caused by above normal water containment inside the reservoir.

1.5.Design Basis

Computational fluid dynamic studies have shown the harvestable capacity of Drop 8, without any modifications to the historic structure, is approximately 50 kW, per drop. This implies a 100 kW potential power capacity at the site. An additional 20 kW generation from the kinetic energy harvested from diffuser action yields the maximum capacity of each drop. As such, the

theoretical maximum capacity of Drop 8 is 140 kW, with 70 kW power available from each drop.

1.6. Anticipated hydropower recovery at EBID Drop 8 structure

Preliminary design parameters for hydropower begins by taking the known parameters of a site, namely discharge and pressure head, and computing a specific speed. Specific speed is expressed either in RPM, or as a dimensionless number. Based upon a theoretical estimate of shaft torque and RPM, the task then is to choose an appropriate generator/alternator such that the plant would operate at its best efficiency point.

There is a large body of information concerning how to compute specific speed for conventional, large hydropower plant design. However, for micro-hydro there is very little information regarding low-head performance of axial-flow reaction turbines.

There are several specific speed formulas and charts suggested in literature to obtain a set of preliminary design parameters. Consider, for example, the chart shown in Figure 6 to determine the specific speed for axial-flow reaction turbines. At the maximum efficiency of 94%, the efficiency of a Kaplan turbine with variable pitch impeller blades, the specific speed is 135 RPM.

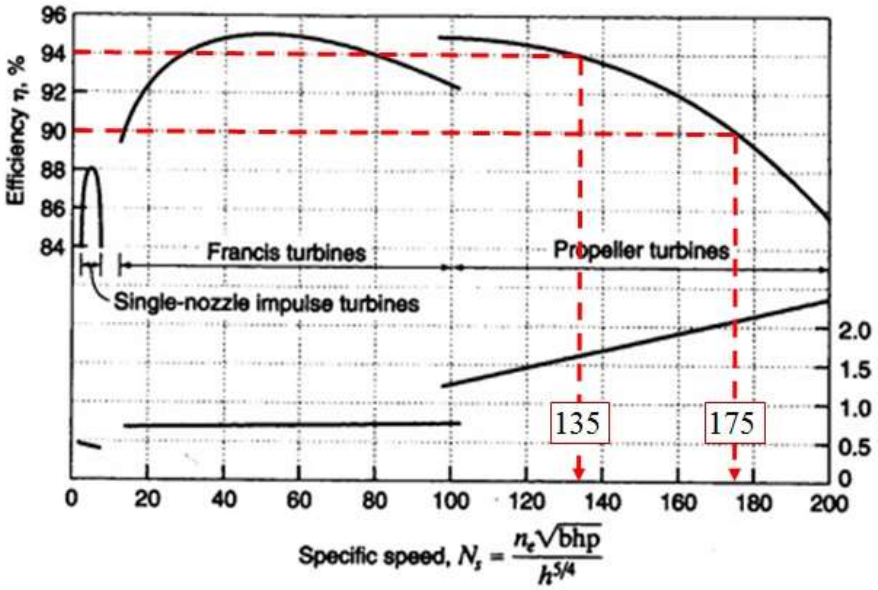

Figure 6. Efficiency vs Specific speed (Moody)

Assuming 90% as the desired efficiency of the HyPER harvester design, we could choose 175 RPM as the speed at which an impeller operates at the best efficiency point. However, since the HyPER harvester has fixed pitch impeller blades it would be operating at lower efficiency. At 85% efficiency Figure 6 indicates the shaft speed is 200 RPM.

Using the chart in Figure 7, on the other hand, the specific speed, for flow parameters at Drop 8 and for head less than 10 feet, would be greater than 200 RPM. This value is beyond the chart range. The logarithmic scale suggests a specific speed close to 400 RPM, if not slightly higher.

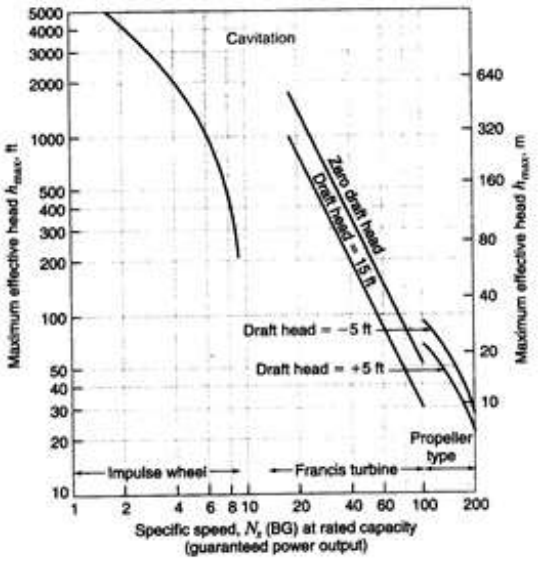

Figure 7. Head vs Specific Speed

Therefore, the question is at what speed can an impeller turn given a pressure head of 2.22m?

Literature search produced a remarkable empirical formula developed by Schweiger and Gregory[1] which yields the relationship between specic speed and pressure head for head less than 2.5 meter. It is a dimensionless number, given by:

Specific speed $N_{sp} = \frac{2.294}{H^{0.486}}$ (1)[2]

At the Drop 8 irrigation structure, the head can vary between a maximum of 2.22 meters to a minimum when the power generation naturally subsides towards the tail-end of the irrigation season. We assume around 1 meter as the minimum pressure head to continue producing power. From a design perspective, this head would be approximately equal to the length between the Venturi inlet and the impeller. The impeller is approximately 1 meter below the drop when the reservoir is full and water is at the maximum height of 1.22 meters above the drop. During low-

[1] Schweiger, F. and Gregory, J. "Developments in the design of Kaplan turbines" Water Power & Dam Construction, Vol. 39, #11, Nov. 1987, pp. 16-20.]

[2] The USBR suggests $N_{sp} = 2.716/H^{0.5} = 2.716/2.22^{0.5} = 1.823$. This yields approximately 14-18% higher figures than Schweiger and Gregory. It is reasonable, therefore, to consider Schweiger and Gregory as a conservative basis for the design parameters.

flow conditions the head above the drop inside the reservoir is small. Variation in the effective head above an impeller is illustrated in Figure 8.

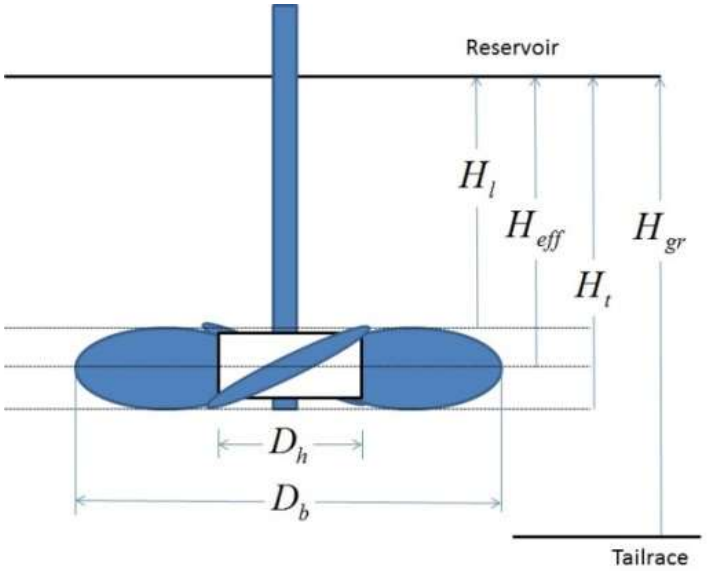

Figure 8. Head above the impeller

The specific speed versus head relationship is computed for the expected range of pressure head variation and is illustrated in Figure 9.

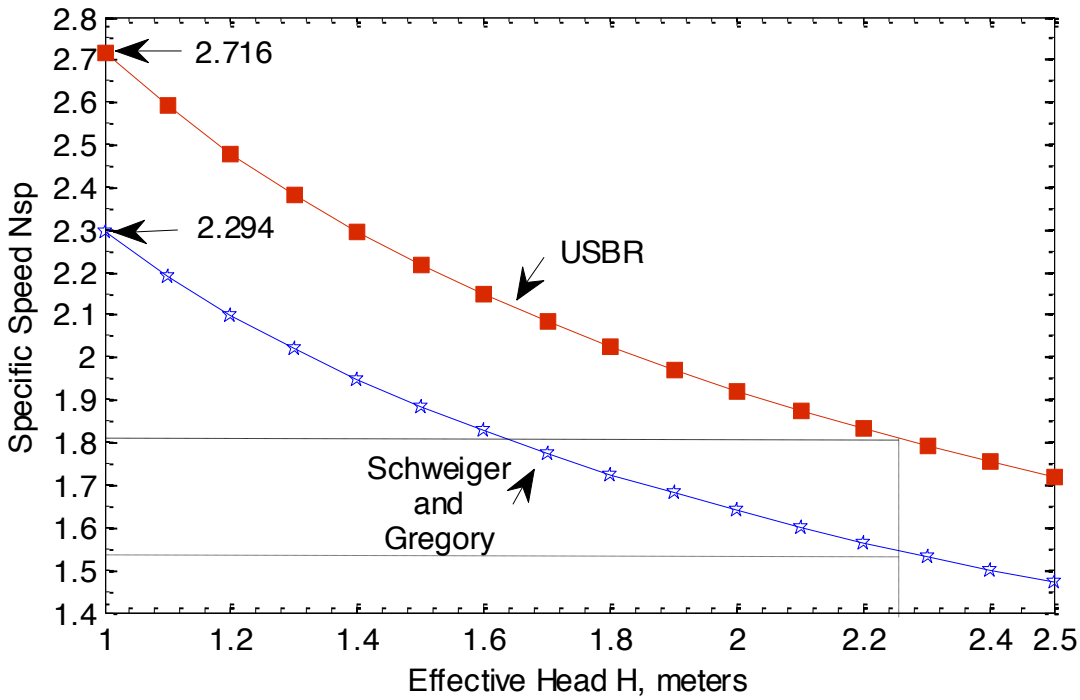

Figure 9. Specific Speed vs Head (Comparison between USBR and Schweiger & Gregory recommended formulas for specific speed)

This empirical relationship relating specific speed to head is convenient as it allows a direct computation of expected shaft speed from a power source.[3]

The actual discharge from the orifice depends on the cavity formed by the Venturi-turbine and the submarine assembly in the flow path. The actual maximum discharge obtained from CFD simulations yield the mass-flow rate through the harvester $\dot{M} = 3{,}500\,kg/s$. Based on this discharge the following calculations show the amount of power that can be harvested.

With a gross head $H_{gr} = 2.22\ m$ (from water surface in the reservoir to the water surface in the tail race), and assuming the efficiency $\eta = 80\%$, the available power

$$P_{avail} = \eta\,\rho\,Q\,g\,H_{gr} = \eta\,\dot{M}\,g\,H_{gr} = 0.8\times 3500\times 9{,}81\times 2.22 = 60{,}979\,Watts \approx 61\,kW$$

Based on the specific speed and the available power, the shaft speed may be computed as:

$$\text{Shaft speed } N = \frac{N_{sp}(gH)^{1.25}}{\sqrt{P_{avail}}} \qquad (2)$$

Upon substituting for specific speed and available power, it is easy to see that Equation (2) reduces to a function of head and the mass-flow rate.

For example, at a pressure head of 2.22 meters, the specific speed is computed as:

$$N_{sp} = \frac{2.294}{H^{0.486}} = \frac{2.294}{2.22^{0.486}} = 1.557$$

With approximately 68 kW of available power, the shaft speed

$$N = \frac{N_{sp}(gH)^{1.25}}{\sqrt{P_{avail}}} = \frac{1.557\times(9.81\times 2.22)^{1.25}}{\sqrt{61}} = 9.3788\,rev/s, or\ 563\,RPM, or\ 58.929\,rads/\sec$$

Figure 11-13 show the range of shaft speed and available power considering change in the effective head in the range of 0.5-2.5 meters, with a energy conversion efficiency of 90%.[4]

[3] The estimated capacity of Drop 8 is approximately 140 kW (70 kW per drop). It is well understood that not all of this power can be extracted as it would conflict with the Laws of Conservation. As such, the maximum power that can be harvested will be significantly lower than what is available.

[4] The recommendation by Mr. Bickford is to use 75-80% as a more conservative estimate of the conversion efficiency. Naturally, with no changes to the existig infrastructure it is reasonable to expect lower output that at the 90% efficiency target.

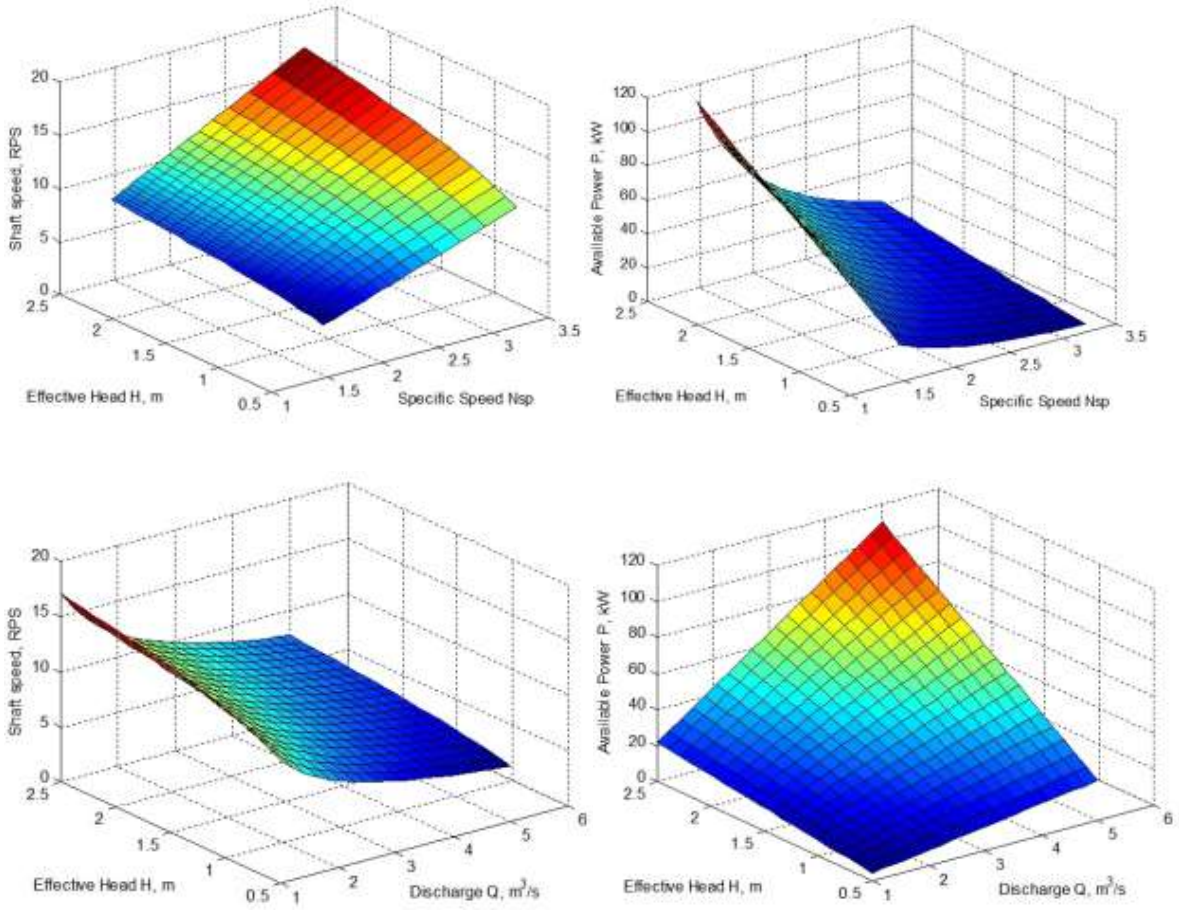

Figure 11. Shaft speed and Available power vs effective head and discharge

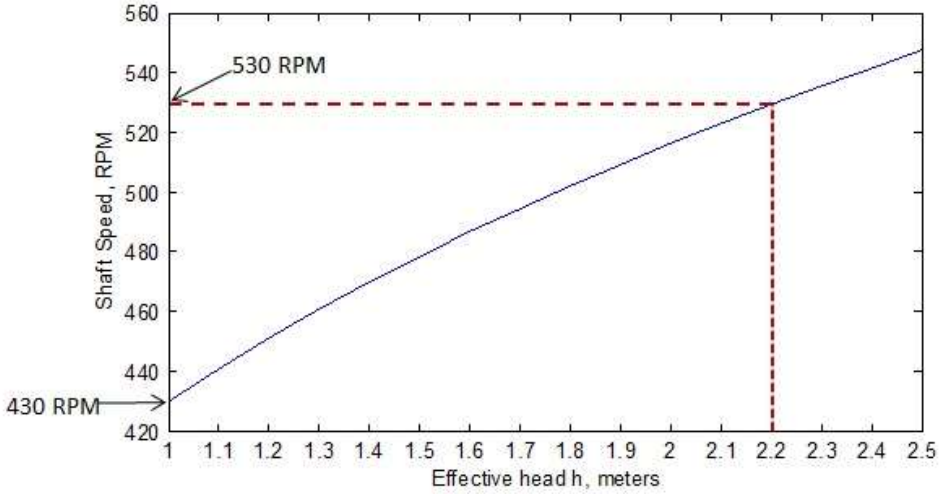

Figure 12. Shaft speed vs head

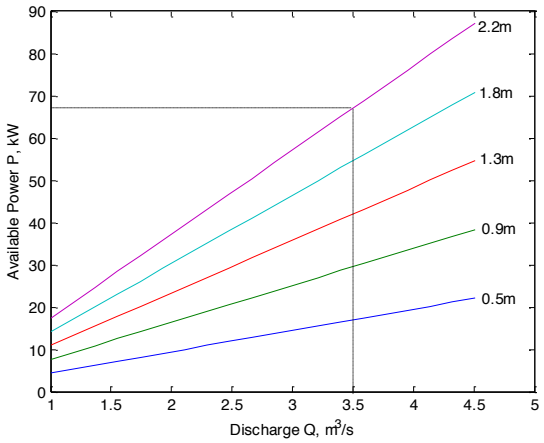

Figure 13. Available power vs discharge for change in head

1.7. Criteria for Selecting Hub-Tip Ratio

An empirical formula suggested by Schweiger and Gregory to compute the runner diameter is given by:

$$D_{Runner} = 84.5(0.79 + 1.602N_{sp})\frac{\sqrt{H_{Effective}}}{60 * \Omega}$$

Where Ω is the angular velocity in rads/sec.

For an effective head of 2.22 meters, the specific speed is 1.557. Assuming a shaft speed of 300 RPM (angular velocity of 5 RPS or 31.42 rads/sec), the runner diameter is:

$$D_{Runner} = 84.5(0.79 + 1.602 \times 1.557)\frac{\sqrt{2.22}}{60 * 31.42} = 0.22\ m\ or\ 8.64"\ diameter.$$

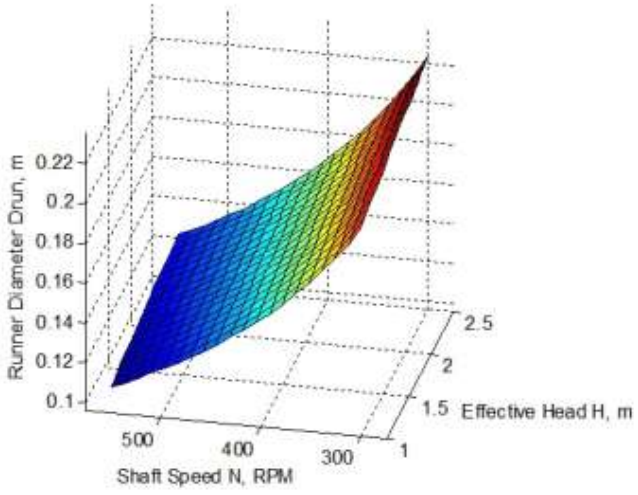

Th diameter computed is impractical because the criteria for hub-tip ratio would require a generator with small overall diameter which may be very difficult to find.

The design concept is to adapt the size of the venturi turbine to any suitable commercially available, off-the-shelf generating component. As such, the basis to select the throat diameter of the Venturi is the overall diameter of the "best" suited generator for the specific application. This is a major criteria for assembling off-the-shelf generators/alternators. The reliability of special generating equipment is costly and make the harvester less affordable. Generators presently manufactured for use in wind generation can be easily adopted.

The design considers two possible Hub-Tip ratios, namely 0.3 and 0.42, that have been investigated and reported in literature. The hub diameter is based on the overall diameter of the generator. In this case, the selection of a low-speed high torque permanent magnet alternator provides the overall diameter. The submarine shell which encloses the generator is optimized for a close fit. The hub diameter, therefore, is the overall diameter of the submarine enclosure. Figure 14 below shows the relative size of the submarine in relation to the hub. Choosing the hub-tip ratio then yields the throat diameter of the Venturi.

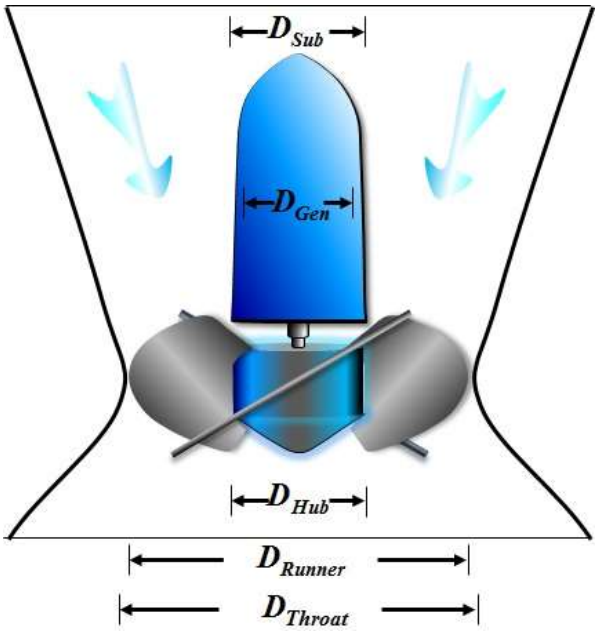

Figure 14. Hub-to-Runner ratio

The constraint posed by Drop 8 is the height of the Venturi. This height must fit the gap between the concrete cylindrical gates above the drops and the floor of the reservoir. As such, the Venturi is designed as a half-hyperboloid and the conical diffusor portion of the Venturi is made part of entry to the suction tube elbow.

$$D_{Hub} = D_{Sub}$$

$$D_{Hub} / D_{Runner} = 0.3 \; or \; 0.42$$

$$D_{Throat} = D_{Runner} + \Delta D$$

$\Delta D/2$ is the gap between the impeller tip and the venturi wall. This gap will be approximately 0.125" – 0.25" depending upon how close the tolerances can be met at the time of fabrication[5].

Naturally, for small hub-tip ratios the blade area is large and the diameter of the Venturi outlet will increase. Conversely, as the ratio increases the effective blade area decreases.

Hub-tip ratio of 0.3

The hub diameter $D_h = 0.32\ m$ based on a generator selection. This takes into account the Carbon composite shell surrounding the generator.

Blade diameter $D_b = 1.07\ m$ based on the hub-tip ratio of 0.3.

Axial fluid velocity $V_a = \frac{Q}{A_{blade}} = \frac{4*\dot{M}}{\rho*\pi*(D_b^2 - D_h^2)} = \frac{4*3500}{1000*\pi*(1.07^2 - 0.32^2)} = 4.275\ m/s$

Angular velocity of the blades based on 533 RPM shaft speed is:

$$U = \omega r = 2\pi N \frac{D_b}{2} = \pi N D_b = \pi * 8.883 * 1.07 = 29.86\ m/s$$

Based on head at the leading edge of the blade $H_l = 1.8\ m$

Tangential velocity at the leading edge $V_{tl} = \frac{gH_l}{U} = \frac{9.81*1.80}{29.86} = 0.5914\ m/s$

Based on head at the trailing edge of the blade $H_t = 2.22\ m$

Tangential velocity at the trailing edge $V_{tt} = \frac{gH_t}{U} = \frac{9.81*2.22}{29.86} = 0.7293\ m/s$

Shaft torque is computed based on the Euler turbine equation, as:

$$\tau = \dot{M}(V_{tt}r_t - V_{tl}r_l) = \dot{M}\frac{D_b}{2}(V_{tt} - V_{tl}) = 3500 * \frac{1.07}{2}(0.7293 - 0.5914) = 258.22\ Nm$$

Shaft power $P_{shaft} = \omega\tau = 2\pi N\tau = 2 * \pi * 8.883 * 258.22 = 14{,}412\ Watts, or\ 14.4\ kW$

Note that the design strategy is to enable easy assembly while keeping all components at their minimum weight. As such the size and weight of the impeller is of concern.

Hub-tip ratio 0.42

For a hub-tip ratio of 0.42, the hub diameter is still $D_h = 0.32\ m$

Blade diameter $D_b = 0.762\ m$

[5] The original design suggested a gap of approximately 1 cm (0.3937"). Reviewer has suggested a gap between 0.125"(min) – 0.25"(max). We will fabricate the device to the lowest tolerance possible without exceeding the maximum recommended. While there is no design change per se, the manufacturing tolerances will be adjusted to reflect this recommended change.

Axial fluid velocity $V_a = \frac{Q}{A_{blade}} = \frac{4*\dot{M}}{\rho*\pi*(D_b^2 - D_h^2)} = \frac{4*3500}{1000*\pi*(0.762^2 - 0.32^2)} = 9.32\, m/s$

Blade angular velocity $U = \omega r = 2\pi N \frac{D_b}{2} = \pi N D_b = \pi * 8.883 * 0.762 = 21.26\ m/s$

Head at leading edge of blade $H_l = 1.8\, m$

Tangential velocity at the leading edge $V_{tl} = \frac{gH_l}{U} = \frac{9.81*1.80}{21.26} = 0.8306\, m/s$

Head at trailing edge of blade $H_t = 2.22\, m$

Tangential velocity at the trailing edge $V_{tt} = \frac{gH_t}{U} = \frac{9.81*2.22}{21.26} = 1.024\, m/s$

Shaft Torque

$\tau = \dot{M}(V_{tt} r_t - V_{tl} r_l) = \dot{M} \frac{D_b}{2}(V_{tt} - V_{tl}) = 3500 * \frac{0.762}{2}(1.024 - 0.8306) = 258.40\ Nm$

Shaft power $P_{shaft} = \omega\tau = 2\pi N\tau = 2 * \pi * 8.883 * 258.40 = 14{,}422\ Watts, or\ 14.42\ kW$

Results indicate hardly any change in power output between the two hub ratios considered. The torque-speed characteristic for hub-tip ratio of 0.42 is shown in Figure 15.

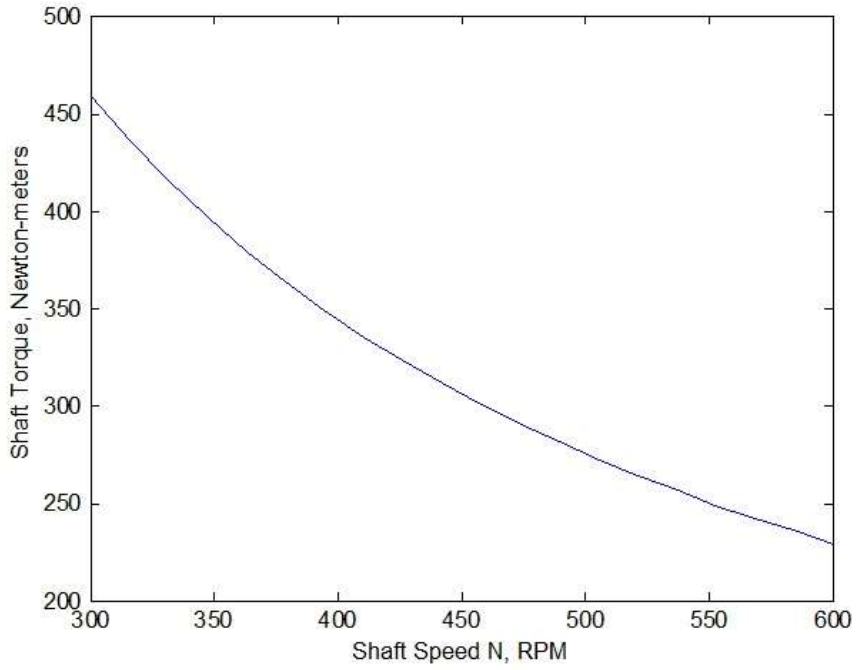

Figure 15. Torque vs Shaft speed

From a physical size perspective, a smaller hub-to-tip ratio increases the runner diameter and hence the throat diameter of the Venturi. This makes the inlet of the suction tube and elbow to be larger in size and conflict with the physical constraints of the Drop 8 structure. A larger diameter impeller weighs more, and costs more.

With physical constraints where there is no possibility for structural modification, an optimal size must be selected. As such, the design is based on a hub-tip ratio of 0.42, as it makes the havester fit better at the Drop 8 site, while providing sufficient margin for implementing successfully.

1.8. Guidevanes

Guide vanes are used to enhance the swirl of the flow approaching the impeller blades. The impeller blades change the tangential velocity component of the flow, and it is this change in tangential momentum that produces the torque that drives the generator. There is also an axial component of force on the blades, produced by the pressure differential across the blades.
If the swirl or tangential velocity component given to the flow by the guide vanes balances the change in tangential velocity through the blades, the flow will leave the blades with zero tangential velocity, i.e., the flow will be purely axial. Theoretically, this is the most efficient operating point since the tangential velocity cannot be recovered as a pressure drop in the draft tube. However, some exit swirl may cause improved performance, for example the flow may follow the diverging draft tube walls better.

If the change in tangential velocity through the blades is not large the increase in efficiency with guide vanes fitted may not justify the extra complications in manufacture, i.e., the turbine could be made with a simpler inlet structure.[6] For ease in fabrication, the guide vanes are oriented at an angle of 90^{o} to the blade angle.

1.9. Impeller design

The runner is the rotating part of the turbine. It includes the hub, blades and shaft. The objective in the harvester design is to minimize the manufacturing cost by simplifying the design features. For example, the use of flat blades with a slight curvature at the tip is easier to manufacture than a curved blade with complex surface geometry. In light of this, a 4-blade impeller with a fixed pitch blade angle is chosen for design. While typically the impeller is made of steel, it could be fabricated as a Carbon composite molding due to its lightweight. However, fabricating the negative mold might not be cost-effective. The mechanical engineering design review recommends the impeller to be made of cast ASTM A743 Steel CA6NM and fabricated as a single piece using a 5-axis CNC machine. Having high impact strength, Type CA6NM an iron-chromium-nickel-molybdenum alloy is resistant to cavitation effects and erosion from silt in the water. For material properties of CA6NM please click: http://www.sfsa.org/sfsa/pubs/hbk/s8.pdf

Ideally, the blade angles at their leading and trailing edges should match the relative flow direction at all radii. This would require complicated curvature of the blades for a non-free vortex approach flow. The blade angle should change from leading to trailing edge and with varying radius. Employing flat blades gives the turbine greater range of application possibilities,

[6] Mr. Bickford recommends guidevanve to be placed at the inlet to the Venturi with 8-12 blades and extending down the length of the Venturi. While this is a very good recommendation, fabrication of a cavity formed with helical guidevanes will be extremely complex and would require 3D printing technology. In fact, as the reviewer has recommended, the Venturi could be fabricated as a single unit. The submarine housing the generator and impeller can be easily inserted and fixed into place. These are future possibilities when the cost of manufacturing can make it affordable to use 3D printing. It appears reasonable to proceed with the simpler approach as designed.

since the manufacture would be less complicated. The runner could be easily fabricated with commonly available machine-shop tools.

The ideal change in angle from leading edge to trailing edge is determined by the change in tangential velocity component that is required. Referring to Figure 13, from the velocity triangle for a flow having axial and tangential velocity components V_{Axial} and V_{Tan}, the angle of the flow β observed relative to a blade moving with tangential velocity $r\omega$, is given by:

$$\tan \beta = \frac{V_{Axial}}{r\omega - V_{Tan}} \qquad (1)$$

Where, $V_{Axial} \approx Q/A$, Q is the discharge and A is the area of cross-section at the throat of the Venturi.

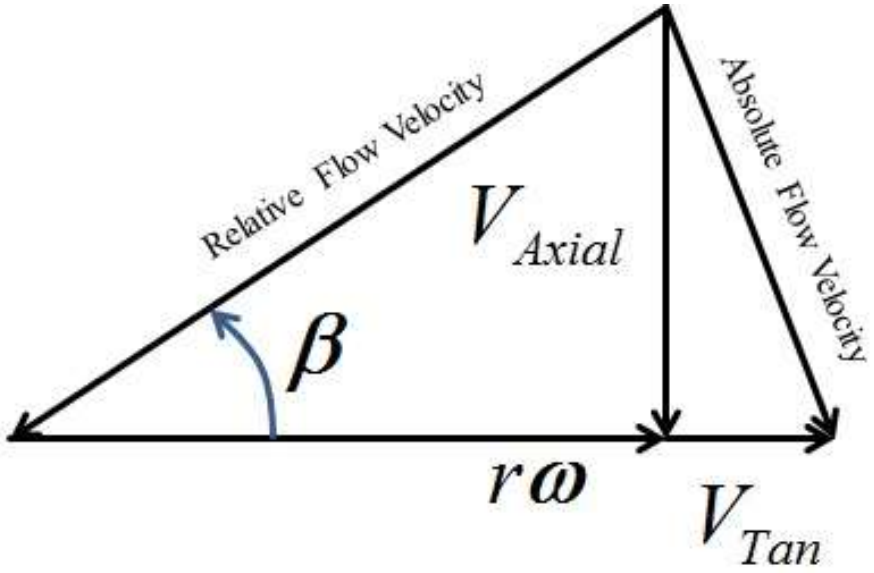

Figure 13. Velocity triangle for blade angle estimation

V_{Tan} is calculated from the change in tangential momentum that yields the required power output. By equating the power produced by the turbine to the rate of change of momentum yields:

$$\eta \rho Q g h = \rho Q \Delta V_{Tan} \qquad (2)$$

Assuming $V_{Tan} = 0$ at the trailing edge so that there is no swirl at the outlet, the leading edge

$$V_{Tan} = \Delta V_{Tan} \qquad (3)$$

The condition assumed in Equation (3) is a simplification to obtain the ideal blade angle. While the swirl created by the trailing edge of the blade must be a minimum, it is reasonable from a

manufacturing viewpoint to adopt a flat blade with a curved tip. The design is to place flat blades at an angle of 30^o with the tips curved up at 15^o. CFD simulations combined with model testing are indeed the only way to design blades having complex geometry. Simulations help in shaping the blade geometry to a load profile which yields the desired performance characteristics.

Substituting Equation (3) in (2) yields $V_{Tan} = \frac{\eta\, g\, h}{r\, \omega}$, which is the swirl velocity introduced by the guidevanes on the runner.

Given an impeller configuration, the effective blade area is computed by:

$$A = \pi\, \frac{(D_{Runner}^2 - D_{Hub}^2)}{4} = \frac{\pi}{4} D_{Runner}^2 \left[1 - \frac{D_{Hub}^2}{D_{Runner}^2}\right]$$

For a set of typical values: With $\eta = 0.9$; $h = 2.22\, m$; $Q = 3.5\, m^3/s$; $D_{Runner} = 0.762\, m$

$$\frac{D_{Hub}}{D_{Runner}} = 0.42$$

$$A = \frac{\pi}{4}(0.762)^2 \times \left[1 - (0.42)^2\right] = 0.3756\, m^2;\ r = 0.3810\, m;\ N = 430\, RPM;$$

$$\omega = \frac{2\pi\, N}{60} = 2\pi \times \frac{430}{60} = 45.03\ rads/s$$

Axial velocity is approximated by:

$$V_{Axial} \approx Q/A$$
$$= \frac{3.5}{0.3756} = 9.3186\, m/s$$

Tangential velocity $V_{Tan} = \frac{\eta\, g\, h}{r\, \omega} = \frac{0.9 \times 9.81 \times 2.22}{0.3810 \times 45.03} = 1.1425\, m/s$

Using Equation (1) $\tan\beta = \frac{V_{Axial}}{r\omega - V_{Tan}}$

$\beta = \tan^{-1}\left[\frac{V_{Axial}}{r\omega - V_{Tan}}\right] = \tan^{-1}\left[\frac{9.3186}{17.156 - 1.1425}\right] = 30.2^o$ angle with respect to the shaft axis.

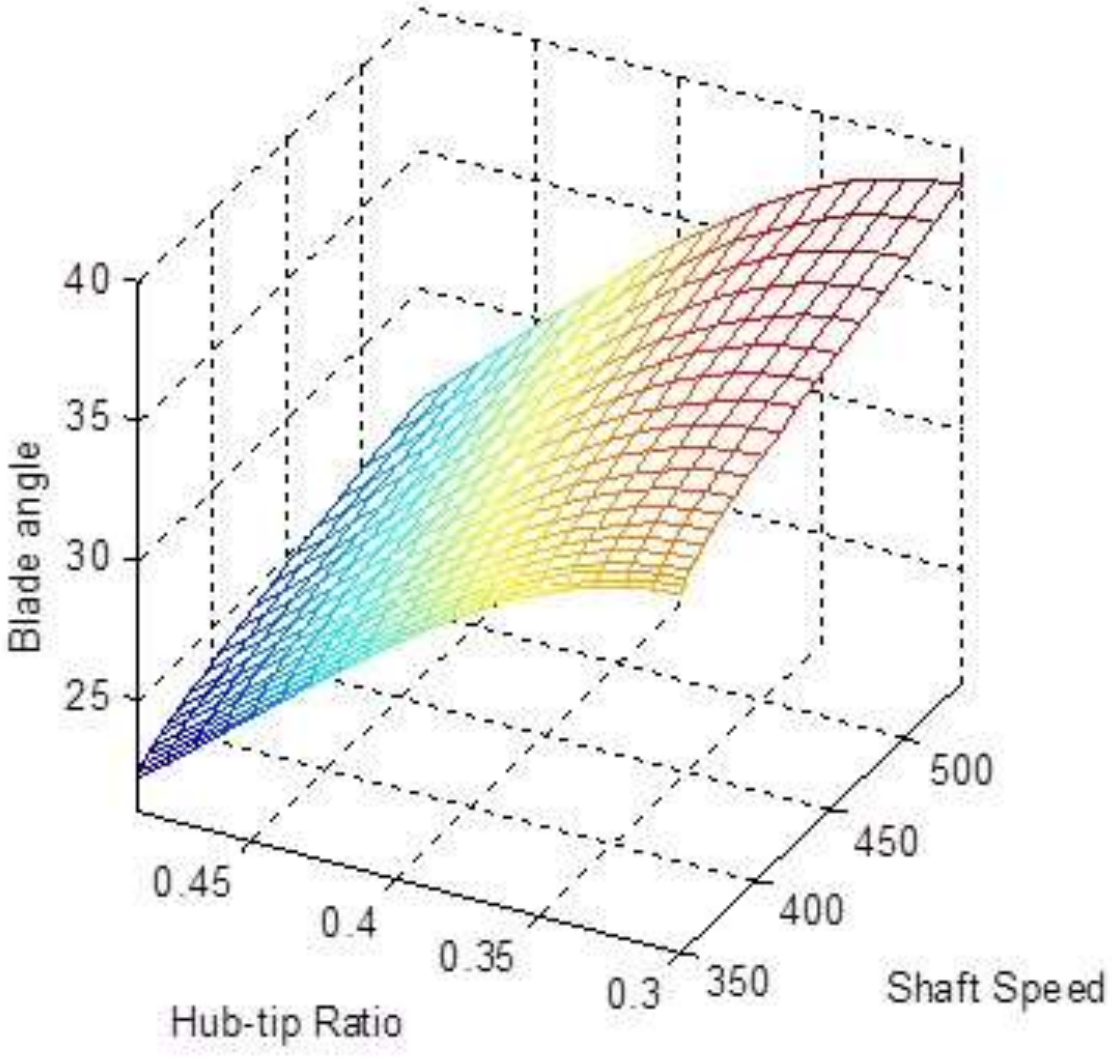

The plot showing blade angle as a function of shaft speed and hub-tip ratio reveals that the maximum blade angle is 38.6^0 over the range of shaft speed of interest. For a hub-tip ratio of 0.42, the best angle is approximately 30^0.[7]

CFD simulations show that the two drops have vortex flow. Because of the structural symmetry, as water enters the inlet gates and flows towards the drops, the flows form swirls in opposite directions. This is important to note because the water that is entering the Venturi has a significant swirl velocity. The cavity formed by the Venturi and submarine is such that flow entering the hyperboloid shaped duct continues to swirl at higher velocity as it exits the Venturi

[7] The recommendation from the Mechanical engineering review is to increase the blade angle to 33 degrees. This is based upon the reviewers design experience with the operation of a low-head hydropower plant at Rock Island with 10 MW units operating at a head of 34.5 feet.

throat. The shape of the Venturi, therefore, aids water discharge through the harvester at high velocity. Simulation shows swirl velocity around 8 m/s at the inlet of both drops.

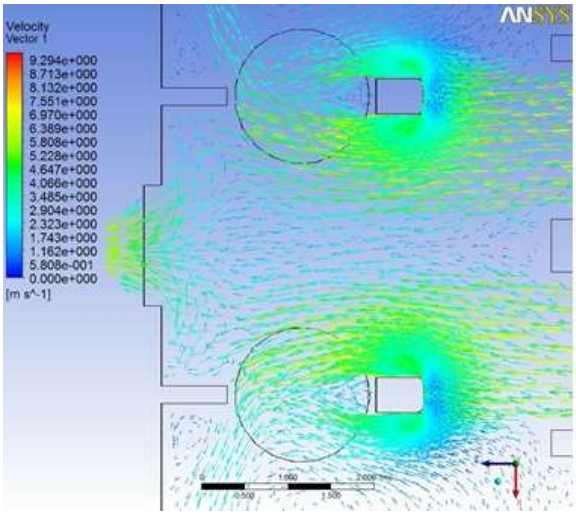

Velocity vectors showing swirl at top surface of water in reservoir above drops

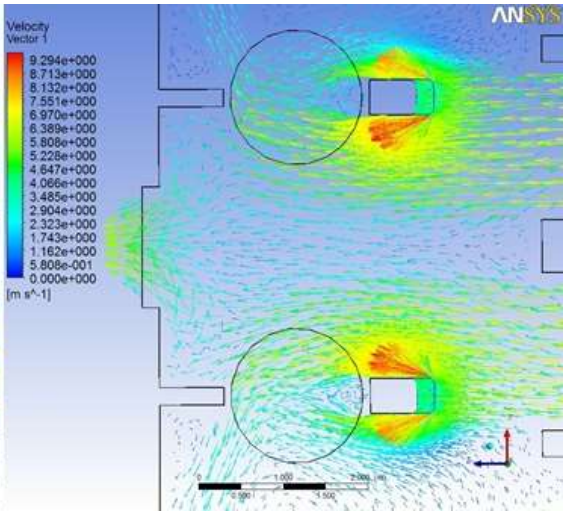

Velocity vectors showing swirl at bottom surface of water in reservoir above drops

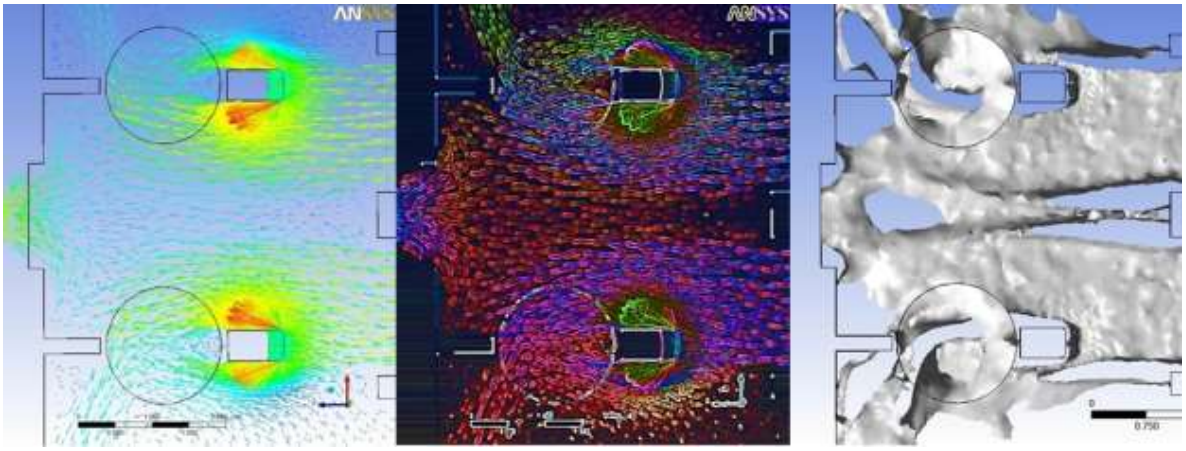

Flow visualization at the bottom of the reservoir showing swirls in opposite directions

In order to take advantage of the higher velocity produced by vortex flow, the impeller motion of each harvester is set to occur in the same direction as the swirl. Guidevanes in each harvester are mounted so as to allow the water to impinge on the leading edge of the blades at maximum velocity.[8] This has the tendency to increase the shaft speed and hence increase the shaft torque.

[8] The reviewer has recommended guidevanes to be placed at the entrance to the Venturi. We will evaluate this in relation to the swirl flow which naturally exists at the drop inlets. The nozzle formed by the submarine should be sufficient to force the water through the guidevanes placed just above the impeller.

4.10. Thrust bearing selection

The vertical-axis implementation requires a thrust bearing for the alternator. The bearing must withstand an axial force caused by the impeller weight, and the force of fluid pressure acting on the blade face.

Impeller mass $20\,kg\ or\ 44\,lbs$

Choosing a ratio of $(D_{Hub}/D_{Runner}) = 0.4$, with $D_{Hub} = 0.32\,m, D_{Runner} = 0.8\,m$

The effective surface area of the impeller blades exposed to pressure head is computed as:

$$A_{eff} = \frac{\pi D_{Runner}^2}{4} - \frac{\pi D_{Hub}^2}{4} = \frac{\pi}{4}(D_{Runner}^2 - D_{Hub}^2) = \frac{\pi}{4}(0.8^2 - 0.32^2) = 0.4222\,m^2, or\ 4.5448\,ft^2$$

Pressure at a depth $h\ meters$ is $P_h = P_{Atm} + \rho\, g\, h$, where $P_{Atm} = 101.325\,kPa$, $\rho \approx 1000 kg/m^3$, and $g = 9.81\,m/\sec^2$.

At a depth $h = 1.5\,m\ or\ 4.9213\,ft$ the ideal pressure

$$P_h = 101.325\times10^3 + 1000\times 9.81\times 1.5 = 116{,}040\,Pa, or\ 1.1833\,\mathrm{kg/cm^2} = 16.8302\,psi$$

From CFD simulations, average pressure drop across impeller $1.0545 kgf/cm^2\ or\ 15\,lbsf/in^2$

The net axial force acting on the impeller blade is

$$F_{axial} = (1.0545 kgf/cm^2)(0.4222\times10^4\,cm^2) = 4452.1\,kgf\ or\ 9815.2\,lbsf$$

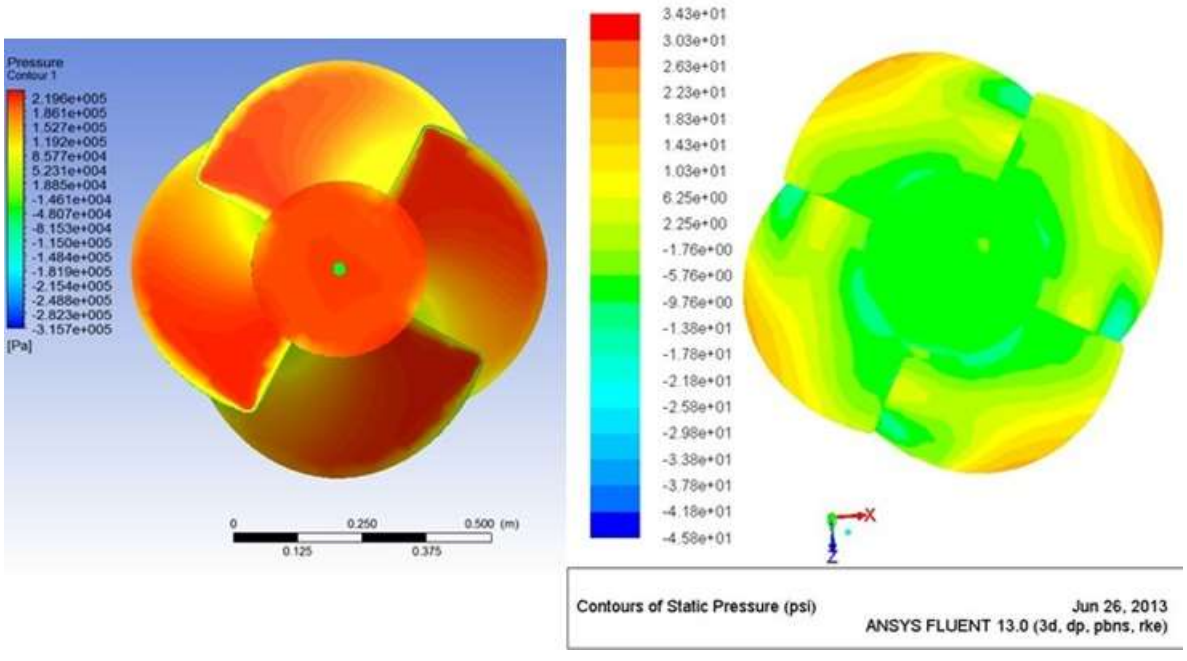

Figure shows the pressure acting on the face and back of impeller blades.

1.10. CFD simulations of the complete harvester system

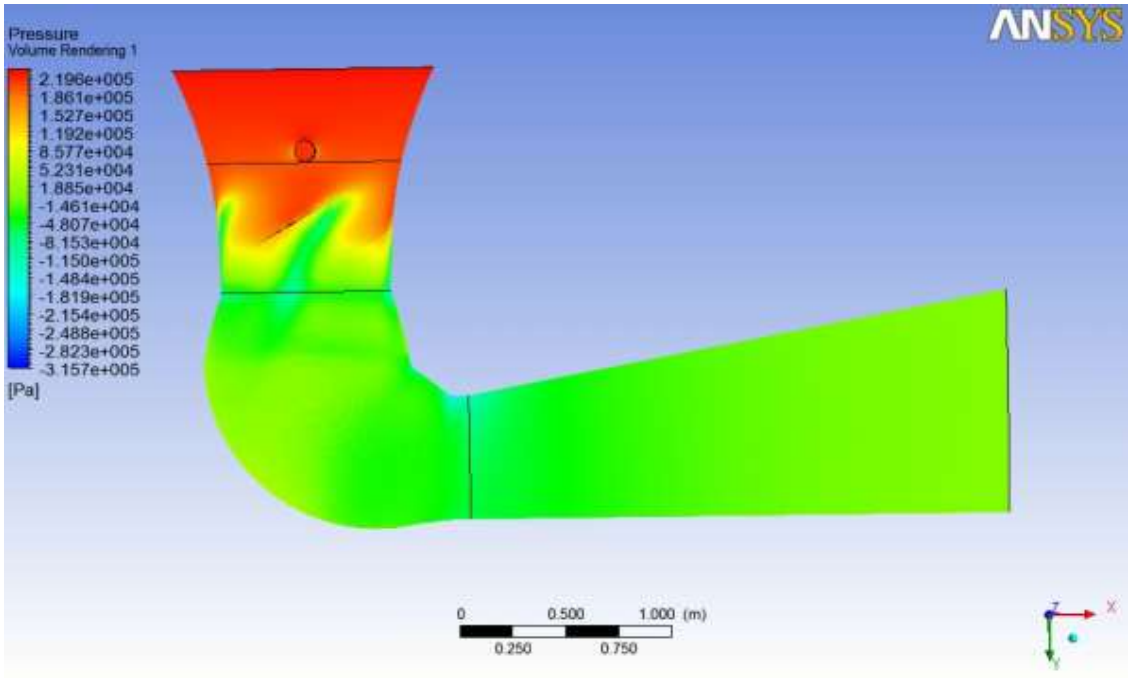

Pressure profile for mass-flow rate of 3500 kg/sec

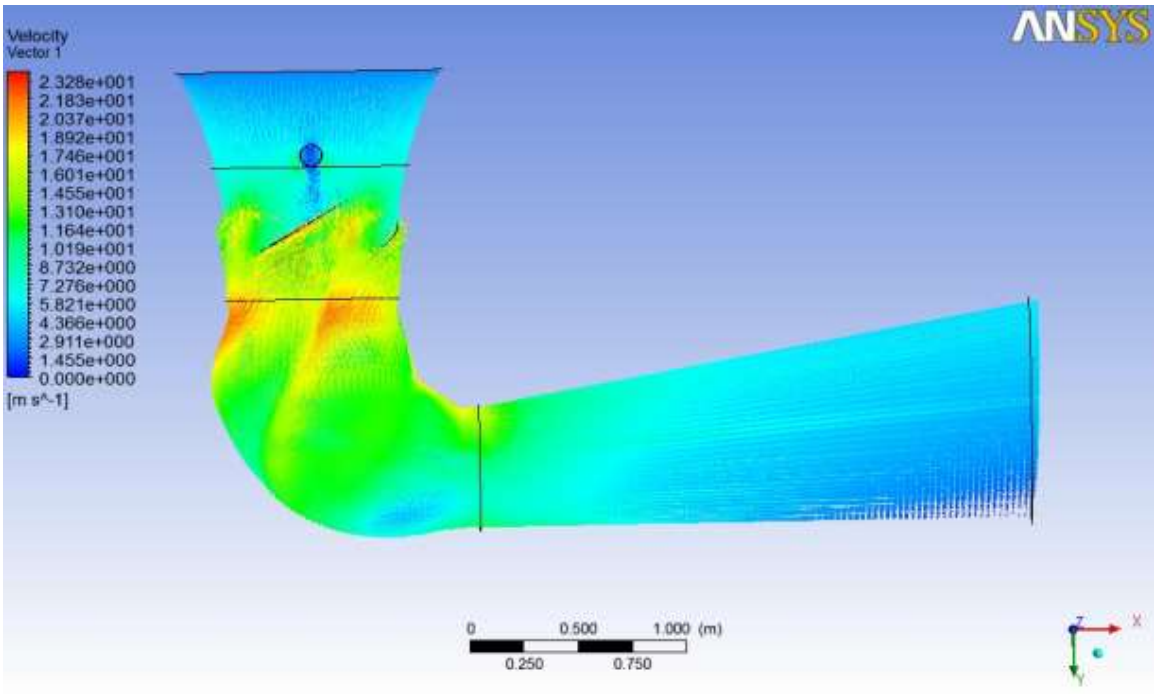

Velocity profile for mass-flow rate of 3500 kg/sec

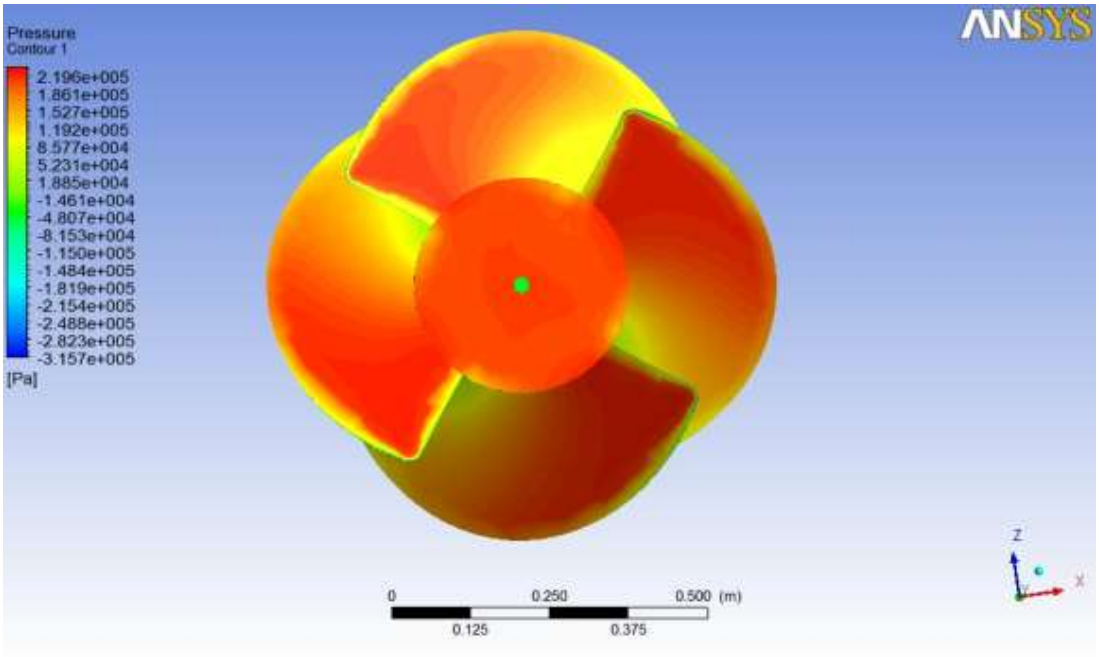

Static pressure contours on front face of impeller

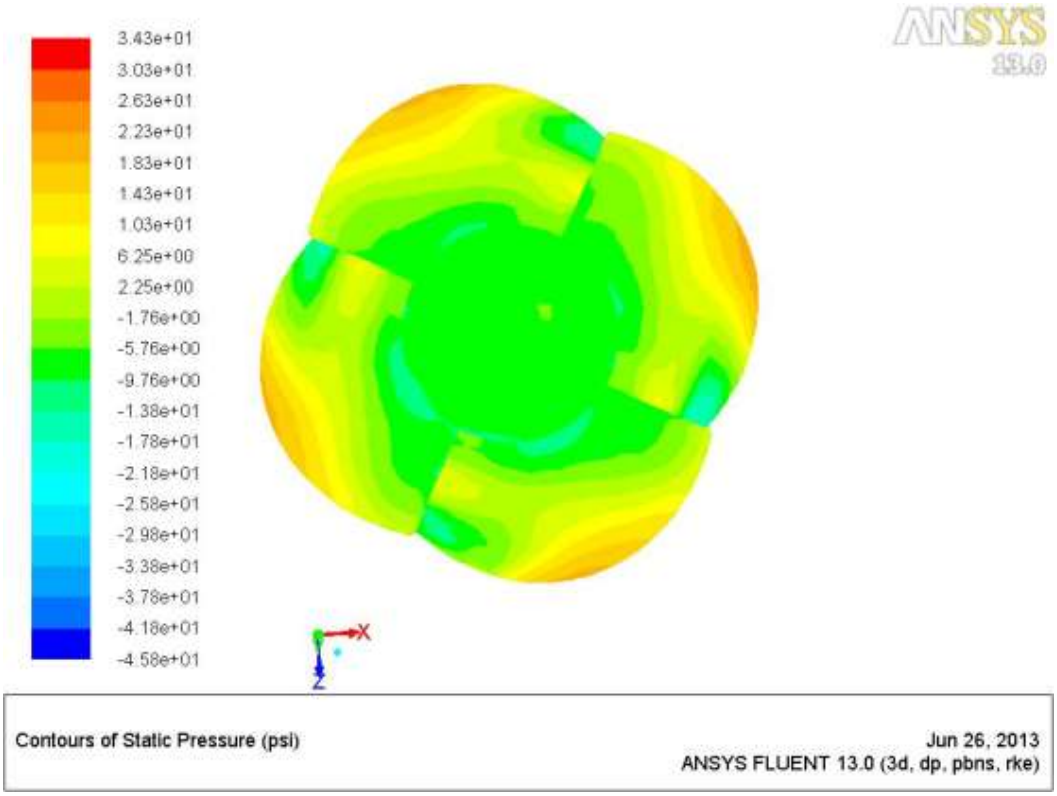

Static pressure on back face of impeller

2. Conclusions

At the maximum efficiency of 94% (the efficiency of a variable-pitch propeller driven Kaplan turbine), CFD studies have shown the maximum harvesting potential is 27 kW without any modifications to the Drop 8 structure. However, with fixed blades while conversion efficiency can be as low as 75-80% there is sufficient confidence that the proposed objective of harvesting 20 kW will be met from two, one of a kind, 10 kW hydropower prototypes.

Simplicity in design and packaging of elements leads to substantial cost reductions in manufacturing and assembling hydropower harvesters. A plug-and-play modular architecture makes the installation easy and helps in creating a robust market for a new generation of hydropower harvesting systems. The self-supporting structure lowers the LCOE thereby making it an affordable technology. With strong commercialization possibilities, the HyPER harvester holds promise towards its expanded use worldwide for hydropower generation from low-head water resources.

Scalability is observed in the ratio of input to output discharge. By appropriate choice of Venturi throat diameter for known inlet velocity and area of cross-section, the outlet velocity can be fixed to the desired value. The height of the Venturi is optimized to the drop by considering the suction tube elbow and draft tube relative to the Venturi-turbine. In principle, the volumetric size of the suction tube elbow must be equal to the discharge capacity of the Venturi.

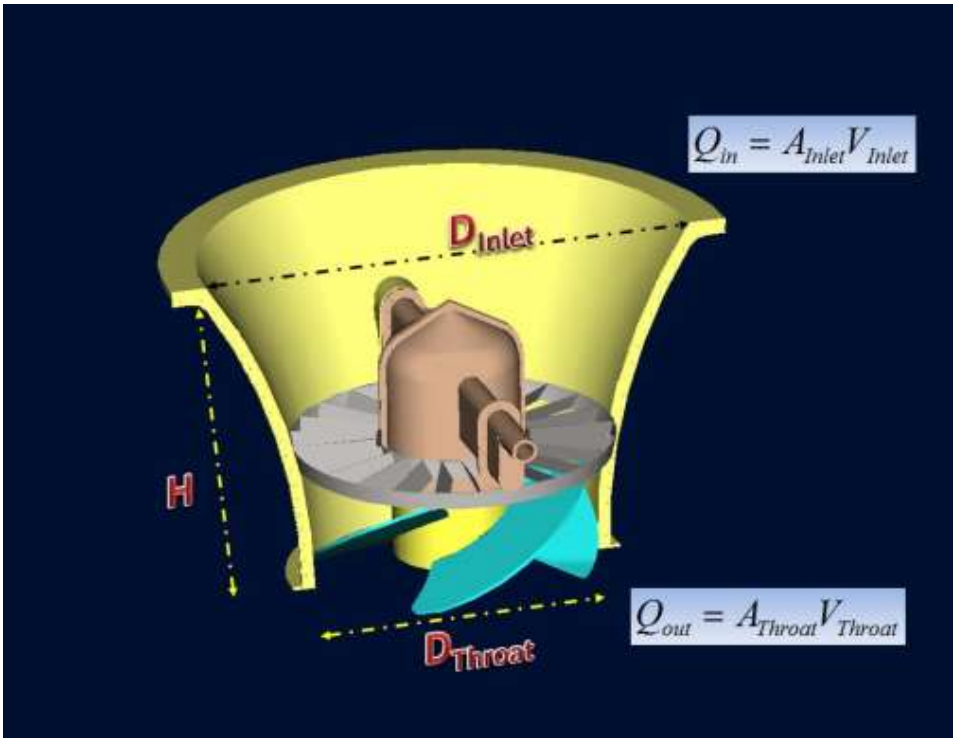

References

1. "Micro-hydropower: Reviewing an old concept" DOE/ET/01752-1, January 1979 http://hydropower.inel.gov/techtransfer/pdfs/doe-et-01752-1.pdf.
2. Boucher, P. J. "Chutes-de-la-Chaudiere: optimizing hydraulic potential, enhancing natural beauty" Hydro Review, Vol. XX, #4, July 2001, pp. 76-80.
3. Gordon, J. L. "Turbine selection for small low-head hydro developments", Unknown publishing date. http://www.hallandsvkrf.se/litteratur/workshops/Turbine%20selection%20for%20small%20low%20head%20hydro.pdf

For sizing turbine water passages after obtaining the turbine runner size:-

4. USBR Engineering monograph No. 20 "Selecting hydraulic reaction turbines", http://www.usbr.gov/pmts/hydraulics_lab/pubs/EM/EM20.pdf
5. Schweiger, F. and Gregory, J. "Developments in the design of Kaplan turbines" Water Power & Dam Construction, Vol. 39, #11, Nov. 1987, pp 16-20.
6. Sadek, R. and Sinbel, M. A. "Water turbines and dimensional analysis" Water Power Vol. 12, #10, Oct. 1960, pp 381-389.
7. Rock Island Unit efficiency curves: B10 (test result with 33 degree blade angle), B9 (simulated result with 36 degree blade angle)

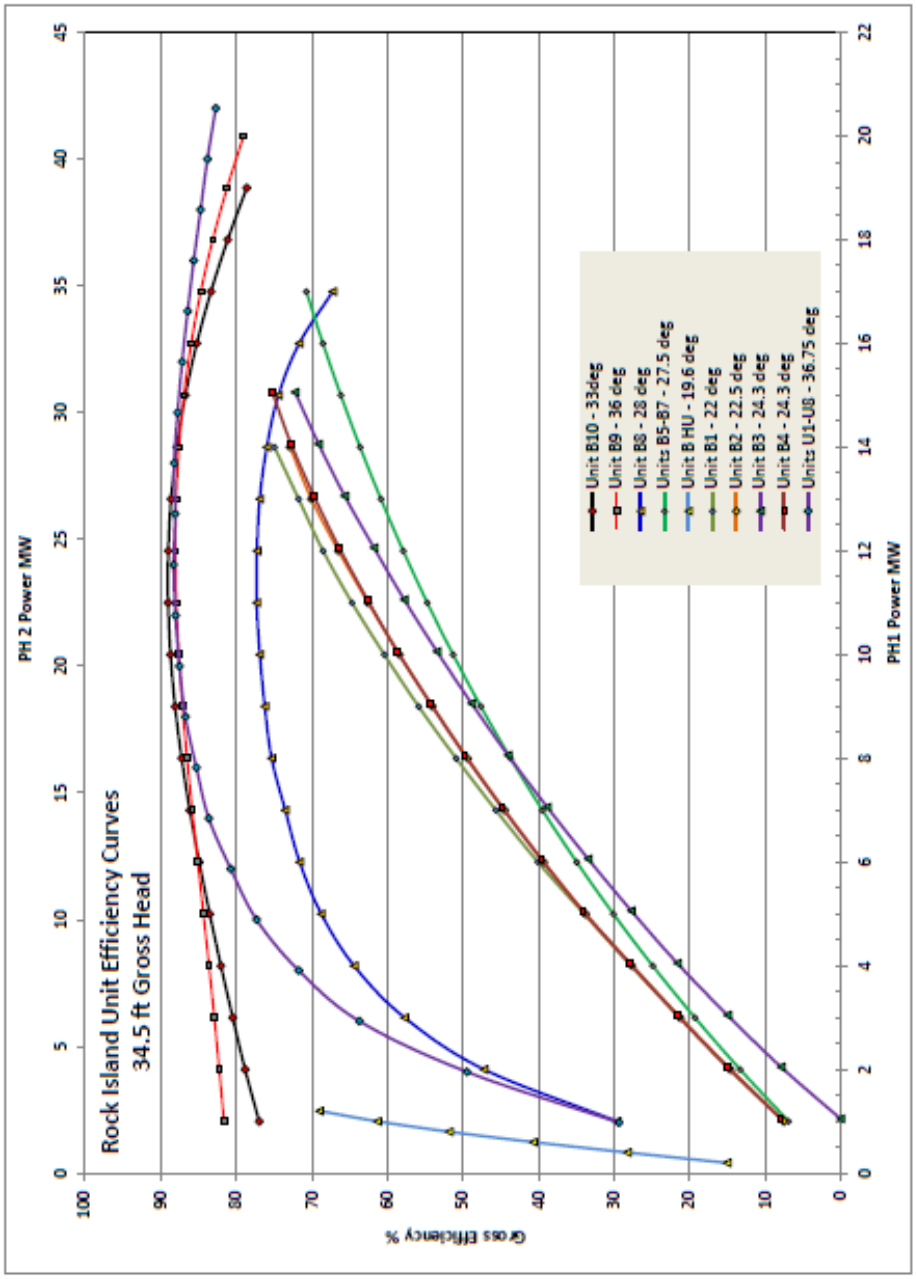

8. Recommended Draft tube design features

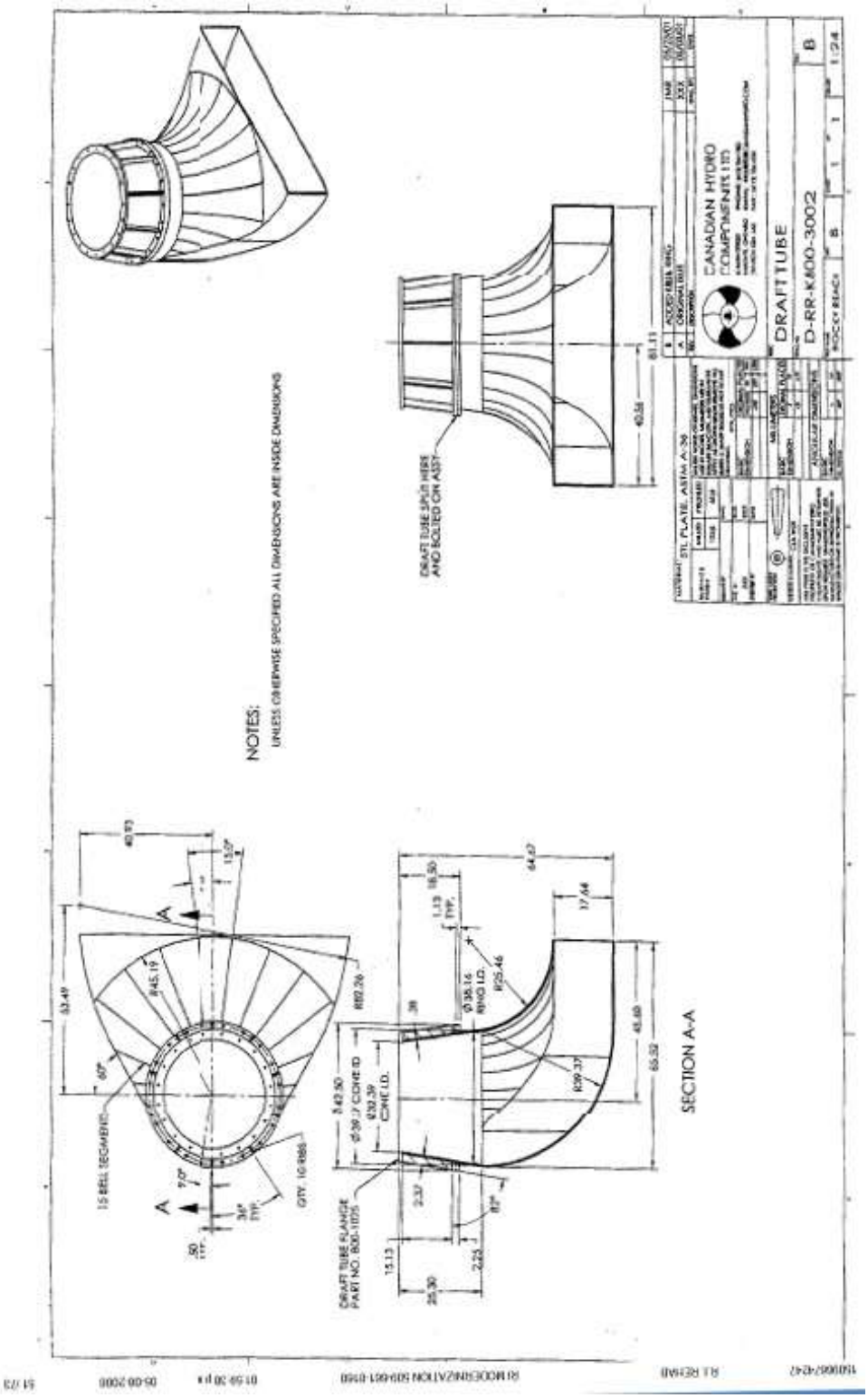

9. Guidevanes and general assemly of Kaplan turbine

10. 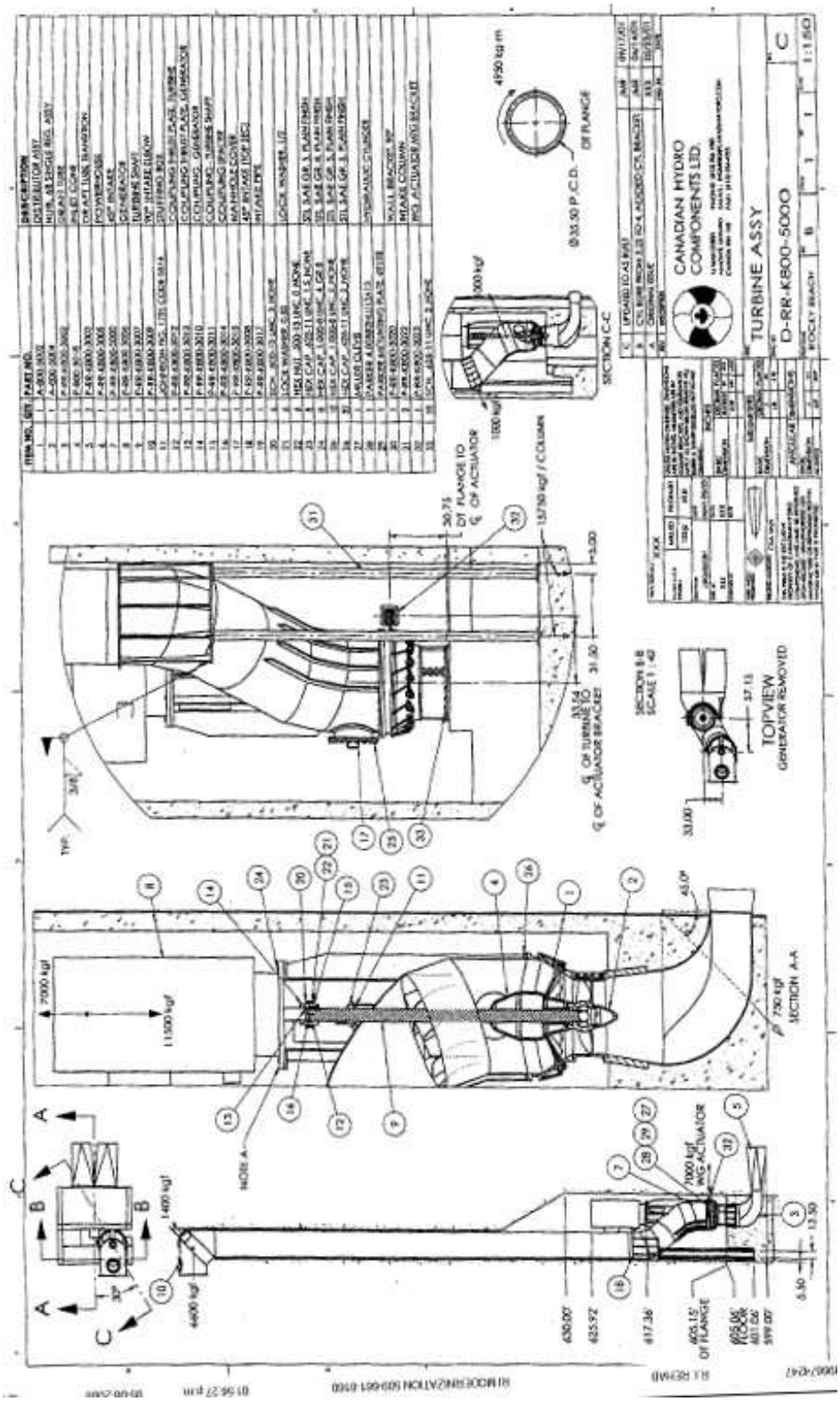
CANADIAN HYDRO COMPONENTS LTD.
TURBINE ASSY
D-RR-K800-5000
TOP VIEW
GENERATOR REMOVED
SECTION A-A
SECTION C-C
SECTION B-B
SCALE 1:40